CHAPTER 3

3.0 COAL AND CHAR CHARACTERISATION

3.1 Introduction

This chapter presents detailed characterisations and results thereof, of the parent coal and subsequent char samples required to relate the fundamental coal and char properties to the CO_2 reactivity of the chars. Several techniques, both conventional (proximate and ultimate analysis, total sulphur content and calorific value determination) and advanced (XRD and XRF) were used.

Detailed petrographic analysis (organic composition and reflectance properties) was conducted on the samples. This provided both a detailed maceral analysis of all the coal samples; and char carbon forms and structural and textural analysis of the chars. Various physical structural properties of the parent coal and char samples were also determined using surface area and pore size analyser and helium pycnometry (HP). The origin of the coal samples, methodologies and procedures of the various characterisation techniques are also discussed.

3.2 Origin of Coal Samples

The four original coal samples used in this study, identified for confidentiality purposes as coal samples; B, C, C2 and D2, were supplied by Eskom and originated from mines in the Highveld area. The parent coal samples were received in particle sizes ranging from fine powder to 5 *cm*.

3.3 Sample Preparation

Mechanical size reduction was employed to reduce the particle size of the coal samples as received to the required size ranges for various analyses and char preparation. For each coal sample, 300 g of the +5 *mm* size fraction was separated and crushed with a jaw-crusher (Samuel Osborne (SA) LTD, Model: 66YROLL) set at maximum jaw opening initially to gradually reduce the particle size. The crushed sample was screened with a 1.7 *mm* screen; then the jaw opening was decreased slightly and the top-size coal particles from the 1.7 *mm* screen were passed through again. This process was repeated until the entire 300 g sample passes through the 1.7 *mm* screen.

Further size reduction of the -1.7 *mm* particle size, was conducted using a Fritsch P-14 rotary mill (R-mill) with a mounted 280x230mm macro crusher (Model No. 46-126) containing 10mm ceramic balls. The speed setting used was 600 rpm and the mill was allowed to run for 30 minutes. Samples were screened as necessary to remove the required particle size fraction and crushing continued. It should be noted that the mill

was cleaned properly with compressed air prior to use to avoid any contamination with previous crushed samples. The different size fractions were then weighed out into 30 g samples which were flushed with nitrogen and appropriately sealed in vacuumed bags to prevent oxidation.

The particle size requirements for the various analyses and the char production as well as the screens used to achieve these are given in Table 3.1.

Table 3.1: Size requirements for coal and char characterisation analyses.

Analysis technique	**Size requirement (µm)**	**Screen used (µm)**
Char production	1000 <dp<1120	1120;1000
Petrography	"	"
HP measurements	"	"
Gas adsorption	"	"
Proximate analysis	75<dp<212	212; 75
Ultimate analysis	"	"
Total sulphur analysis	"	"
CV determination	"	"
XRD mineral analysis	<75	75
Demineralisation	"	"
XRD carbon fraction analysis	"	"

3.4 Char Preparation at 900 ℃

The already screened required size fraction of parent coals (1000 <dp<1120 µm), was used to produce the chars. This was done by the Coal Research Group, North-West University.

3.4.1 Charring Apparatus and Procedure

The char production was conducted in a Packed Bed Balance Reactor (PBBR). The schematic representation of the reactor is shown in Figure 3.1. The PBBR consists of a vertical tubular furnace mounted on a very sensitive microbalance by an aluminum tripod. Nitrogen gas was purged through the bottom of the reactor at a flow rate of 1500 $cm^3 \cdot min^{-1}$ as measured by a gas flow controller. The temperature in the furnace was controlled by a programmable heat controller attached to the furnace unit. The furnace can be programmed to work both isothermally and non-isothermally (ramp). The weight loss due to devolatilisation was observed via an online data acquisition module with the attainment of a constant weight taken as indicative of the completion of the char production process.

This PBBR is dedicated to char production and is capable of handling up to 60 *grams* of sample per batch. Char production in a separate and dedicated reactor prior to TGA experiment was done in order to prevent the condensation of tars and volatiles on the delicate TGA as noted by Kaitano (2007). The char production conditions are given in Table 3.2

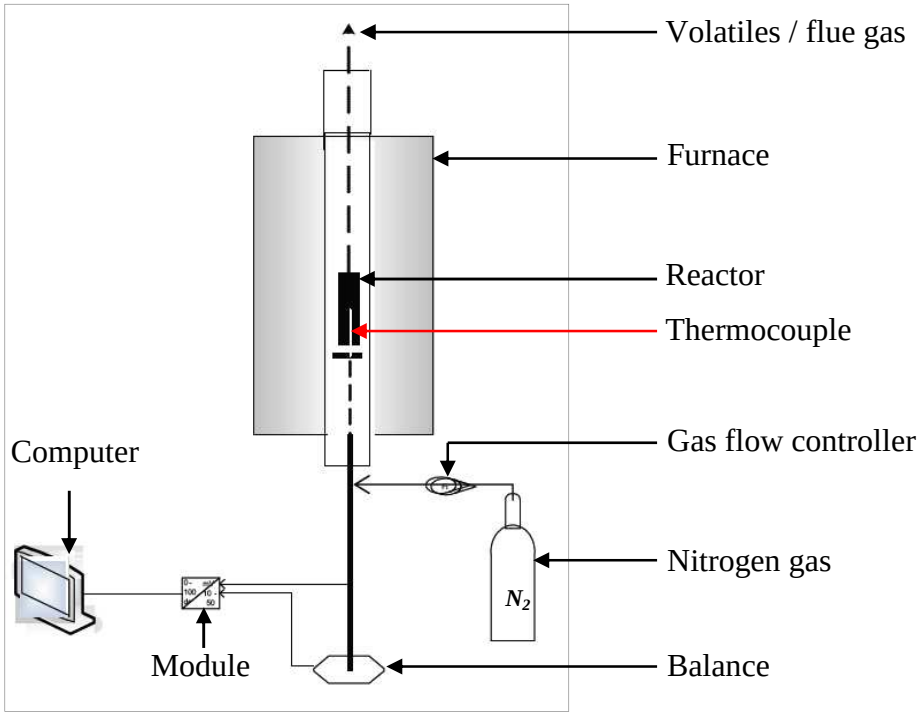

Figure 3.1: Experimental setup for char preparation (Not drawn to scale)

(Kaitano, 2007)

Table 3.2: Char production conditions.

Char production conditions	
Mass of coal per batch	60 *g* (maximum)
Initial ramp	20 $℃{\cdot}min^{-1}$
Final isothermal temperature	900 *℃*
Holding time	70 *min*

The char production sequence from the parent coal samples are as follows: The coal samples were sieved into the required 1*mm* average particle size and put in an oven at 60 *℃* for 1 *hour* to drive off condensed moisture. The sample temperature was equilibrated to ambient temperature and pressure in a flow of nitrogen.

It was then heated non-isothermally at 20 $℃{\cdot}min^{-1}$ in a nitrogen atmosphere to the target temperature of 900 *℃* and then, held isothermally at the target temperature for 70 minutes. A final constant weight showed that all the volatiles had been driven off. The furnace was then turned off and the sample cooled down to ambient temperature and pressure under nitrogen flow. After cooling, the samples were analysed for char yields and packaged in vacuumed plastic bags under nitrogen flow with the labels: Char B, Char C, Char C2 and Char D2.

The char samples to be used for XRD carbon crystallite and XRF ash components analyses were prepared further. They were pulverized to -75 μm and demineralization was done on part of them as required by XRD carbon analysis. The samples to be used for TGA experimentation were split to fractions of 50 ± 1 *mg* using a rotary sample splitter at a speed of 10 rpm. Fully prepared and or split char samples were stored in a dessicator from which samples were taken for various analyses as well as for experiments on the TGA.

The result of the char yield after devolatilisation of the precursor coals is presented in Table 3.3. It can be seen from the char yield data that the moisture and volatile matter content of the parent coal (based on proximate analysis of the coals (*adb*)) are almost driven off completely. Discrepancies in the total percentage is probably due to the presence of traces of volatiles still trapped in the char as was confirmed from the proximate analysis (Table 3.8).

Table 3.3: Char yield after production.

Char Yield				
Char ID	**B**	**C**	**C2**	**D2**
Char yield (*wt. %, adb*)	73.5	75.6	78.9	72.4
Moisture and VM of parent coal (*wt. %, adb*)	27.3	24.8	21.1	28.1
Total (*wt. %, adb*)	100.8	100.4	100	100.5

3.5 Coal and Char Characterisation Analyses

The various characterisation analyses conducted on the four coal and four intermediate char samples, including the laboratories they were conducted at, are summarised in Table 3.4.

Table 3.4: Characterisation analyses conducted on the coal and char samples.

Analysis	**Property**	**Laboratory Used**
Chemical & Mineralogical	Proximate	Advanced Coal Technology / NWU
	Ultimate	Advanced Coal Technology
	Calorific value	Advanced Coal Technology
	Total sulphur	Advanced Coal Technology
	Mineral (XRD)	University of Pretoria
	Ash (XRF)	Council for Geosciences, Pretoria
Petrographic	Maceral composition	Petrographics SA
	Vitrinite reflectance	Petrographics SA
	Carbon-mineral Structure	Petrographics SA
	Char form	Petrographics SA
Structural	Carbon crystallite (XRD)	PANalytical XRD, Randburg
	Gas adsorption (CO_2)	North-West University
	HP measurements	North-West University

3.6 Coal and Char Characterisation Equipment and Techniques

3.6.1 Chemical Analyses

Chemical analyses of the samples comprised of proximate and ultimate analyses; calorific value analysis; and total sulphur content determination. The proximate analysis on all the four char samples was done at the North-West University, while that of the parent coals was done at the Laboratory of Advanced Coal Technology (ACT) Pretoria. The ultimate and total sulphur analysis of all the samples was also done at ACT according to the standard methods shown in Table 3.5 (du Cann, 2007 and 2008).

Table 3.5: Analytical methods used for chemical and mineralogical analysis.

Items	Standard Method
Sample Preparation	SABS 0135: Part 1 & 2. (1997)
Proximate Analysis	
Inherent Moisture Content (%)	SABS 925
Ash Content (%)	SABS ISO 1171 (1997)
Volatile Matter Content (%)	SABS ISO 562 (1998)
Fixed carbon Content (%)	By Difference
Ultimate Analysis	
Carbon (%)	ISO 12902
Hydrogen (%)	ISO 12902
Nitrogen (%)	ISO 12902
Oxygen (%)	By Difference
Total Sulphur Content (IR Spectroscopy) (%)	ISO 19759
Calorific Value ($MJ.Kg^{-1}$)	SABS ISO 1928 (1995)
Grade (Based on CV, Air dry basis)	CKS 561-1982
Mineralogical Analysis	
Ash Analysis (XRF)	ASTM 3682

3.6.2 X-ray Diffraction (XRD) Mineral Analysis

X-ray diffraction (XRD) analysis was used to determine and quantify the different minerals contained in the coal and char samples. This mineralogy analysis was done at the Laboratory of the Geology Department, University of Pretoria (courtesy of Dr. Sabine Verryn).

Already prepared coal samples (-75 μm) were used for this analysis. Char samples were further processed to get the required particle size. 40 g of the four char samples (1 mm particles) were milled down to fine powder of -75μm in a Fritsch P-14 rotary ball mill with ceramic balls.

The powdered samples were transferred to suitable sample holders made of aluminium alloy and tamped gently, but thoroughly with the edge of a glass slide. It was important to fill the sample holders and the surplus was sliced off with a glass slide (approximately 50x70mm and 5 mm thick), while simultaneously compressing the samples in the holders. The above procedures were repeated until smooth surfaces of even texture were obtained.

Analysis on the prepared samples was done using a PANalytical X'Pert Pro powder diffractometer with X'Celerator detector and variable divergence- and receiving slits with *Fe* filtered *Co-Kα* radiation. The analysis parameters and settings on XRD system is shown on Table 3.6.

Table 3.6: Analysis parameters and settings on the XRD system for mineral analysis.

Anode material	Cobalt target, λ: Co Kα=1.78901Å
Generator setting	40 kV; 40 *mA*
Angle of scan	$2.0° \leq 2\theta \leq 135°$
Progressive divergence Slit	1.0° (fixed)
Anti-scatter slit	2.0°
Soller slit	0.02 Radian
Scanning	Continuous
Duration of scan	6- 8 hours

The crystalline phases of minerals present in the samples were identified using X'Pert HighScore plus software. The relative phase amounts (weight %) were estimated using the Rietveld method (Autoquan Program). Amorphous phases, if present, were not taken into account in the quantification.

3.6.3 Ash Analysis (XRF)

In a bid to have more insight into the ash compositions of the high ash chars, major element analysis using X-ray Fluorescence (XRF) spectroscopy was conducted on the chars. This was done at the laboratory of the Council for Geosciences, Pretoria according to ASTM 3682 standards.

For better results the already micronised char samples (-75 μm) were used for this analysis. The technique involves initial drying of the fine char samples at a temperature of 110 $^{\circ}C$ until a constant weight was achieved. The dried samples were then calcined in air at a temperature of 500 $^{\circ}C$ for one hour and at 815 $^{\circ}C$ for four hours, in order to determine the Loss on Ignition (LOI) value as well as to drive off water and all organic components and compounds contained in the char samples. The calcined sample was then converted into a solid solution by fusion with lithium tetraborate ($Li_2B_4O_7$), LTB (one gram of the calcined ash to nine grams of LTB).

The prepared solid solution and standard SARM-2, an international syenite certified reference material from *MINTEK* were placed in the sample holders and put in the sample compartment of the XRF spectrometer.

For quantification, the intensity of a characteristic line of the element to be determined was measured and the concentration of the element in the sample was calculated from the measured intensity (Loubser and Verryn, 2008; Matjie, 2008). Coal and char ashes typically contain: Fe, Al, Mg, Mn, V, Ti, Si, Ca, Na, K, P, S and Cr, which are, by default, reported as oxides: Fe_2O_3, Al_2O_3, MgO, MnO, V_2O_3, TiO_2, SiO_2, CaO, Na_2O, K_2O, P_2O_5, SO_3 and Cr_2O_3 (Loubser and Verryn, 2008; Matjie, 2008). Minor and trace element analysis was not done on the samples. The ash chemistry of the parent coal samples was also not determined.

3.6.4 X-ray Diffraction (XRD) Carbon Crystallite Analysis

XRD was also used to study the carbon crystallite properties of both the coal and char samples. XRD analytical techniques have been established as a useful tool in obtaining the structural information of coal and chars (Lu *et al*., 2001; Feng *et al*., 2003; Gupta, 2007).

The pulverised (-75 μm) coal and char samples for this investigation were demineralised to reduce the amount of mineral matter present in them to minimise their influence during quantitative analysis (Lu *et al*., 2001, Maity and Mukherjee, 2006; Van Niekerk, 2008).

The demineralisation was done according to the modified method adapted from literature (Steel and Patrick, 2001; Lu *et al*., 2001; Maity and Mukherjee, 2006; Van Niekerk, 2008). Twenty grams of each sample was added to 80 ml 5M concentrated hydrochloric acid (HCl) in a glass beaker and agitated with a polyethylene coated magnetic stirrer for 24 hours at 450 revolutions per minute (rpm). The acid was separated from the sample by filtration and the precipitate was added to 80 ml 29M (48 *wt. %*) hydrofluoric acid (HF) in a polyethylene beaker and agitated for 24 hours with a polyethylene coated magnetic stirrer at 450 rpm. The acid was again separated by filtration and the precipitate added again to 80 ml 5M hydrochloric acid for another 24 hours under the same conditions as the first HCl leaching. The acid was separated by filtration and the precipitate was washed under a lower pressure atmosphere with ultrapure water. In order to remove the adsorbed HCl from the residual sample particles, large quantity of ultrapure water was used in the rinse stage until the pH of the filtrate corresponded to 7.0. The remaining fully washed acid-treated samples were dried in a vacuum oven at 60 *℃* until a constant weight was obtained. All the samples were flushed with nitrogen and sealed in plastic bags prior to XRD scans.

Proximate analysis was conducted on the demineralised samples to determine the degree of removal of the minerals in the samples. The effectiveness of demineralisation, E_d, was introduced to quantify the extent of demineralisation. It is the ratio of ash removed or 'demineralised' to the original ash content of the sample expressed in percentage:

$$E_d = \left(\frac{A_i - A_f}{A_i} \right) \cdot 100 \qquad (\%) \qquad (3.1)$$

The XRD scans on the demineralised samples were conducted on a PANalytical XRD X'Pert Pro powder diffractometer using *Co Kα* radiation (courtesy of Dr. Sabine Verryn). The analysis parameters and settings on the XRD system for carbon fraction analysis are presented in Table 3.7.

Table 3.7: Analysis parameters and settings on the XRD system for carbon crystallite analysis.

Anode Material	Cobalt, *Co* target
Generator Settings	45 mA, 35 kV
Angle of scan (°2θ)	$4.0^{o} \leq 2\theta \leq 120^{o}$
$K\alpha_1$ (Å)	1.78901
$K\alpha_2$ (Å)	1.7929
K_β (Å)	1.62083
$K\alpha_2$- $K\alpha_1$ ratio	0.5
Step Size (°2θ)	0.017
Scan Step Time (second)	13.335
Scan Type	Continuous
PSD Mode	Scanning
PSD Length (°2θ)	2.12
Divergence Slit Type	Programmable
Divergence Slit Size (mm)	15
Specimen Length (mm)	10
Measurement Temperature (°C)	25
Spinning	Yes

X-ray intensities were measured and recorded automatically by the X'Pert HighScore plus software. The observed intensity in arbitrary units was processed to get the reduced intensity in atomic unit (*a.u*) through the following steps:

- Obtaining the raw diffractogram of the sample.
- Obtaining the diffractogram of the spiked sample with a reference material of known peak (pure silicon was used in this study).
- Combining the two resulting diffractograms (spiked and unspiked) for any shift in peaks and corrections.
- Doing $K\alpha_2$ stripping on the resulting diffractogram to obtain a final diffractogram with X-ray intensity due to the $K\alpha_1$ radiation only.
- Correcting the resulting final diffractogram for polarisation and geometrical factors using the X'Pert HighScore plus application. The absorption factor, A(θ) was also corrected for using the Milberg equation, shown below (Shiraishi and Kobayashi, 1973; Hubbell and Seltzer, 1996).

$$A(\theta) = 1 - \frac{1}{\alpha}(1 - e^{-\alpha}) \tag{3.2}$$

where α is evaluated from:

$$\alpha = 2\rho' \left(\frac{\mu}{\rho}\right).A.\cos ec2\theta \tag{3.3}$$

where $\left(\frac{\mu}{\rho}\right)$ is the mass absorption coefficient for *Co Kα* radiation, and ρ′ is the bulk density of the sample.

- The average carbon crystallite parameters for both the coal and char samples were determined as follows. The interlayer spacing, d_{002}, was determined using Braggs Law (Equation 2.3, Section 2.5.3), while the crystallite height, L_c, and average crystallite diameter, L_a, were evaluated using the Scherrer equation (Equation 2.1 and 2.2). The average number of aromatic layers per carbon crystallite, $N_{ave,}$ was calculated from d_{002} and L_c, using Equation 2.3 (Section 2.4.3).

- The aromaticity, f_a, of the samples was calculated from the area under the d_{002} peak and the γ_{002} side band using a combination of the Origin 6.1 software and the HighScore Plus curve fitting facility.

- By considering that the scattered X-ray intensity is a combination of intensities contributed by the crystalline and amorphous carbon structures (Lu *et al*., 2001), the reduced intensity of the coal and char samples, *I*, in atomic units can be related to the two separate contributions. Thus:

$$I = I_{cr} + I_{am} \tag{3.4}$$

Since the intensity contributed by the fraction of amorphous carbon is constant over the whole scattering region and does not contribute to the peak intensity and is reflected only in the background (Franklin, 1950; Ergun and Tiensuu, 1959; Lu *et al*., 2001), it is related to and equal to the fraction of amorphous carbon, X_A, contained in the samples. Equation 3.5 can thus be rewritten as:

$$I = I_{cr} + X_A \tag{3.5}$$

If only the reflections within the (*002*) peak is considered, as suggested by Warren (1941) and referenced by Franklin (1950), Ergun and Tiensuu (1959) and Lu *et al*. (2001), then:

$$I = I_{002} + X_A \tag{3.6}$$

By plotting the reduced X-ray intensity against s=2Sinθ/λ, the fraction of amorphous carbon, X_A, was evaluated from the symmetrical curve of the d_{002} peak using the relation derived by Franklin (1950):

$$I_{002} = \left(\frac{0.0606}{s^2}\right) \times \sum_n \left(p_n \times \frac{\sin^2(\pi N_{ave} d_{002} s)}{N_{ave} \sin^2(\pi d_{002} s)} \right) \tag{3.7}$$

Combining Equation 3.6 and 3.7 yields:

$$\frac{I_{002}-X_A}{1-X_A}\times\frac{s^2}{0.0606}=\sum_n\left(p_n\times\frac{\sin^2\left(N_{ave}d_{002}\pi\cdot s\right)}{N_{ave}\sin^2\left(d_{002}\pi\cdot s\right)}\right) \tag{3.8}$$

where s=2Sinθ/λ; P_n, is the fraction of aromatic carbon contained within the d_{002} peak.

Since all the carbons within the (*002*) peak is completely crystalline and aromatic, ΣPn=1, and introducing, I_{max}, as the maximum reduced intensity within the (*002*) peak, the solution for the fraction of amorphous carbon now becomes:

$$\frac{I_{\max}-X_A}{1-X_A}=\frac{0.0606}{s^2}\times\frac{\sin^2\left(N_{ave}d_{002}\pi\cdot s\right)}{N_{ave}\sin^2\left(d_{002}\pi\cdot s\right)} \tag{3.9}$$

- The degree of disorder index, *DOI*, of the samples was calculated from the aromaticity, f_a, and the fraction of amorphous carbon, X_A, using the relation (Lu *et al*., 2002a):

$$DOI=X_A+(1-X_A)(1-f_a) \tag{3.10}$$

3.6.5 Petrographic Analysis

The petrographic analyses of all the coal and char samples were done at Petrographics SA, Pretoria (du Cann, 2007 and 2008). These analyses involve the microscopic examination of the samples, which, in conjunction with other techniques, gives the necessary details pertaining to the age or maturity of the coal samples; their organic

composition; the mineral and organic matter associations; and the physical properties and general condition of the samples.

The following analytical methods were used for the analyses. Petrographic block preparation of the samples (parent coals and chars) using epoxy resin was done according to ISO 7404 - 2 (1985) standard. The resulting samples were ground and polished. The samples were then examined under the microscope (Leica DM4500P) under a reflected light oil immersion lens. Vitrinite random reflectance measurements in accordance with the ISO Standard 7404 – 5 method (1994) were conducted in order to establish the rank or degree of maturation of the samples.

The maceral groups (mono-, bi-, and tri-macerals) were quantified by a 500 point-count technique in accordance with the ISO Standard 7404 - 3 method (1994). The reactive inertinite macerals were identified according to Smith, Roux and Steyn for South African coals (Smith *et al.*, 1983). A total maceral reflectance scan was also undertaken on each of the samples (coals and chars). 250 random reflectance readings were taken on all macerals over the polished surface of each petrographic block.

Coal microlithotype, carbominerite and minerite analyses were conducted in accordance with the ISO Standard 7404 - 4 method (1988) to determine the organic/inorganic associations. A condition analysis was also performed on all the coal and char samples using the same 500 point-count technique as in the case of group macerals in order to analyse the extent of visible changes in the organic constituents due to heat treatment by the char production process.

3.6.6 Structural Analysis

Various analyses were conducted on the coal and char samples to ascertain their physical and structural properties. Some of the properties identified for analysis in this study were: the micropore surface area; the average micropore diameter; the skeletal density; the microporosity; and the carbon crystallite microstructural parameters.

3.6.6.1 CO_2 Adsorption Analysis

The micropore surface area of the parent coal and the chars was measured by CO_2 adsorption using the Dubinin- Radushkevich method (Anderson *et al*., 1965; Walker and Kini, 1965; Walker *et al*., 1988) on a Micromeritics ASAP 2020 Accelerated Surface Area and Porosimetry System (Micromeritics, 2006). Carbon dioxide is most commonly to measure micropore surface areas of coals/chars (Anderson *et al*., 1965; Walker and Kini, 1965; Walker *et al*., 1968). Prior to CO_2 adsorption, the samples (about 0.20 grams each) were degassed under vacuum (10.0 μmHg) in order to eliminate any moisture or condensed volatiles that may impede adsorbate accessibility. The degassing of the coal samples was done at ambient temperature (25 $^{\circ}C$) for 48 *hours* to avoid the release of volatiles and the formation of low temperature chars. The chars were degassed at 380 $^{\circ}C$ using a ramp of 2 $^{\circ}C \cdot min^{-1}$ with holding temperatures of 90 $^{\circ}C$ (for 1 *hour*) and 380 $^{\circ}C$ (48 *hours*). The evacuated samples were analysed at 0 $^{\circ}C$ in an ice bath. The results were processed using the ASAP 2020 V3.01 software linked to the facility. The ASAP 2020 uses two independent vacuum systems, one for sample analysis and one for sample preparation. This allows preparation and analysis to proceed simultaneously without the inherent delay found in single vacuum system analyzers that must share a vacuum pump.

The average micropore diameter and micropore volume was determined using the Horvath-Kawazoe (H-K) method (Horvath and Kawazoe, 1983; Jaroniec *et al*., 1996; Kowalczyk *et al*., 2002; Micromeritics, 2006). The porosity of both the coals and the subsequent chars ($D_p \leq 5$Å) was determined using the CO_2 adsorption data. Porosity of a material, usually expressed as a percentage, is the ratio of the total volume of voids available for fluid transmission to the total volume of the porous medium (Webb, 2001; Micromeritics, 2006). To determine the volume of open pores, the cummulative volume of CO_2 adsorbed has to be calculated. This was achieved by integrating the cumulative pore volume over the entire measured pore diameter range. Hence porosity was evaluated using the relation (Webb, 2001; Micromeritics, 2006):

$$\varepsilon_o = \rho_c \int \frac{dV}{dD_{pore}} \cdot dD_{pore} \tag{3.11}$$

3.6.6.2 Helium Pycnometry

The skeletal or apparent density of a solid particle is the ratio of the mass of discrete particles of the solid material to the sum of the volumes of the solid materials and the closed, blind or inaccessible pores within the particles (Gan *et al*., 1972; Strugala, 1994; Webb, 2001).

The determination of the skeletal density of the coal and char samples was conducted using the Quantachrome Stereopycnometer (Model: SPY-4). The pycnometer is manually operated and is specifically designed to measure the true volume of solid materials using the Archimedes principle of fluid (gas) displacement (Helium was used in this study) and the technique of gas expansion (Webb, 2001; Quantachrome Instruments, 2009). From this volume, density is easily determined using the sample mass. It has a digital pressure display resolution of 0.001 *psi* and an error of < 0.2% when properly prepared (both sample and equipment), thermally equilibrated, and when the sample occupies greater than 75% of the nominal sample cell volume (Tamari and Aguilar-Chávez, 2004; Quantachrome Instruments, 2009).

Ideally, a gas is used as the displacing fluid since it needs to penetrate the finest pores to ensure maximum accuracy. Due to both its small atomic dimension, enabling entry into crevices and pores approaching one Angstrom (10^{-10} m), and its behaviour as an ideal gas, helium is recommended and was used in this study. Other gases such as nitrogen can also be used, often with no measurable difference. The pycnometer also offers a choice of two interchangeable sample cells (20 and 135 cm^3) used in conjunction with a single reference volume.

About 10 grams of sample is placed in the 20 cm^3 sample cell and degassed by purging with a flow of helium, by vacuum, or by a series of pressurization cycles. The standard analysis is performed by pressurizing the sample cell to approximately 17 *psi* and recording the value. The selector valve is rotated so the gas expands into the reference or added volume and that lower pressure is recorded. From these two readings, the sample volume can be quickly and accurately calculated (Tamari and Aguilar-Chávez, 2004; Quantachrome Instruments, 2009).

3.7 Characterisation Results and Discussion

3.7.1 Chemical Analyses

Results of proximate, ultimate, and total sulphur analyses, as well as the hydrogen-carbon (H/C) and the oxygen-carbon (O/C) atomic ratios of all the coal and char samples are given in Table 3.8.

From the summary, inherent moisture content of the parent coals ranges from 3.40 *wt. %, adb* for coal C to 6.50 *wt. %, adb* for coal D2. These coals are low in volatile matter (VM) content with coal B, C, C2 and D2 having VM values of 23.3, 21.4, 18.2 and 21.6 *wt. %, adb* respectively. Since the charring process drives away moisture and volatiles in the parent coal resulting in a carbon enriched char, the inherent moisture and volatile matter content of the chars reduced drastically. Moisture content decreased from 4.00 *wt. %, adb* in coal B to 0.90 *wt. %, adb* in char B, while it went down from 6.50 *wt. %, adb* in coal D2 to 0.37 *wt. %, adb* in char D2. Similar downward trends were also observed in chars C and C2.

Volatile matter content also saw the same downward movement with a range of 18.2 to 23.3 *wt. %, adb* in the coals reduced significantly to a very low value range of 0.80 to 2.70 *wt. %, adb* in the chars. Chars have been known to contain traces of moisture and VM matter especially when prepared at temperatures below 1200 *°C*. Several investigators have reported traces of moisture and VM in their chars prepared at or below 1000 *°C* (Dutta *et al*., 1977; Matsui *et al*., 1987; Ochoa *et al*., 2001; Sinağ *et al*., 2003; Zhang *et al*., 2006; Murillo *et al*., 2006; Zhang *et al*., 2007; Everson *et al*., 2008b)

The coals were characterised as high ash coals with approximately equal ash content values of: 25.6, 29.7, 28.6 and 29.0 *wt. %, adb* for coal B, C, C2 and D2 respectively. The chars experienced a corresponding increase in ash content with respective values of 28.5, 33.2, 34.0 and 36.7 *wt. %, adb* for char B, C, C2 and D2. It is worth noting that the approximate ash content of the parent coal was one of the motivations for the selection of these four coal samples for this study.

The fixed carbon content of the coals were: 47.1 *wt. %, adb* for coal B; 45.5 *wt. %, adb* for coal C; 49.4 *wt. %, adb* for coal C2; and 42.9 *wt. %, adb* for coal D2. Fixed carbon content of the chars increased, as should be expected after transiting from coal, to values of 69.4, 64.8, 61.2 and 60.2 *wt. %, adb* for char B, C, C2 and D2 respectively.

The upper heating value of these coals under laboratory conditions on air dry basis, usually referred to as the gross calorific value, are low, with values ranging from 18.1 *MJ/kg* for coal D2 to 21.4 *MJ/kg* for coal B. On a calorific value basis, the four coal samples are graded as Grade D-III coals with all CVs less than 21.5 MJ/kg (CKS 561-1982). These results are similar to those obtained by Kaitano (2007) and Hattingh (2009) in their investigations of some inertinite-rich Highveld coals and discards. Gross calorific value of the four chars was not determined.

The ultimate analyses revealed all four coal samples to be rich in elemental carbon with coals B, C and C2 having 73.1 *wt. %, daf* and coal D2 having the lowest elemental carbon content of 68.1 *wt. %, daf*. This property makes them ideal as feedstock for coal conversion processes as the elemental carbon can complement the heat required for some of the endothermic processes in the gasifier. The slight rank difference of coal D2 (Bituminous medium rank D) was manifest in the elemental carbon content – as elemental carbon content increases with rank (van Krevelen, 1981; Falcon and Snyman, 1986; Kabe *et al*., 2004). Thus, coal D2, being of a slightly lower rank than the other three coals, had the lowest elemental carbon content.

Elemental oxygen content of the coals ranges from 19.0 *wt. %, daf* for coal B to 24.9 *wt. %, daf* for coal D2. Total sulphur content ranges from 0.64 *wt. %, daf* for coal D2 to 1.49 *wt. %, daf* for coal B, and nitrogen content ranges from 1.44 *wt. %, daf* for coal D2 to 1.77 *wt. %, daf* for coal B. On this basis coal D2 should be most desirable environmentally, since it has minimum content of both total sulphur and nitrogen.

The elemental carbon content of the chars increased accordingly to a range of 89.7 *wt. %, daf* for char C2 to 93.1 *wt. %, daf* for char D2, while total sulphur content increased to values of 0.42 to 1.49 *wt. %, daf,* and nitrogen content decreased from parent coals to chars with reported values ranging from 0.07 *wt. %, daf* for char D2 to 0.62 *wt. %, daf* for char B.

Table 3.8: Result of proximate and chemical analyses of coal and char samples.

Proximate Analysis	**Coal B**		**Char B**		**Coal C**		**Char C**		**Coal C2**		**Char C2**		**Coal D2**		**Char D2**	
(*wt. %)*	**adb**	**db**	**adb**	**db**	**adb**	**db**	**adb**	**db**	**adb**	**db**	**adb**	**db**	**adb**	**db**	**adb**	**db**
Inherent Moisture	4.00	-	0.90	-	3.40	-	1.20	-	3.80	-	1.58	-	6.50	-	0.37	-
Volatile Matter, VM	23.3	24.3	1.20	1.21	21.4	22.2	0.80	0.81	18.2	18.9	3.20	3.30	21.6	23.1	2.70	2.70
Ash	25.6	26.7	28.5	28.8	29.7	30.7	33.2	33.6	28.6	29.7	34.0	34.5	29.0	31.1	36.7	36.8
Fixed Carbon, FC	47.1	49.0	69.4	70.0	45.5	47.1	64.8	65.6	49.4	51.3	61.2	62.2	42.9	45.8	60.2	60.5
Total	**100**	**100**	**100**	**100.01**	**100**	**100**	**100**	**100.01**	**100**	**99.9**	**99.98**	**100**	**100**	**100**	**99.97**	**100**
Gross Calorific Value (adb) (MJ/kg)	21.4		-		20.0		-		20.2		-		18.1		-	
Grade (Based on GCV, (adb))	Grade D III		-		Grade D III		-		Grade D III		-		Grade D III		-	
Ultimate Analysis (Ash free basis) (*wt. %*)																
Carbon	70.2	73.1	91.2	92.0	70.6	73.1	90.6	91.7	70.4	73.1	88.3	89.7	63.7	68.1	92.7	93.1
Hydrogen	4.66	4.85	2.02	2.04	4.70	4.83	2.02	2.04	4.30	4.51	2.42	2.45	4.56	4.87	2.22	2.23
Nitrogen	1.71	1.77	0.61	0.62	1.61	1.65	0.29	0.30	1.60	1.67	0.55	0.56	1.34	1.44	0.07	0.07
Oxygen	18.2	19.0	3.80	3.85	18.7	19.4	4.75	4.80	19.5	20.3	6.70	6.80	23.3	24.9	3.54	3.55
Total Sulphur	1.26	1.32	1.47	1.49	0.99	1.02	1.10	1.12	0.40	0.42	0.46	0.49	0.60	0.64	1.05	1.05
Total	**100.03**	**100.04**	**100**	**100**	**100**	**100**	**99.96**	**99.96**	**100**	**100**	**100.01**	**100**	**100**	**99.95**	**99.95**	**100**
H/C atomic ratio	0.792	0.792	0.264	0.264	0.804	0.792	0.264	0.264	0.732	0.744	0.348	0.324	0.852	0.852	0.288	0.288
O/C atomic ratio	0.195	0.195	0.0315	0.0315	0.195	0.195	0.0413	0.039	0.210	0.210	0.057	0.057	0.278	0.278	0.0285	0.0285

The reduction in elemental nitrogen from coal to chars could be attributed to the partitioning and speciation of the coal nitrogen to $NO_{X,}$ which leaves as flue gas with the volatiles. Conversely, the increase in elemental sulphur contents is an indication that sulphur in the studied char samples is primarily bound to the organic matrix and the minerals and therefore, increases proportionally to the evacuation of moisture and volatiles during the devolatilisation reaction.

The hydrogen-carbon (H/C) atomic ratio in the coals ranged from 0.79 for coal B to 0.85 for coal D2 while the oxygen-carbon (O/C) atomic ratio were between 0.20 for coal B and 0.29 for coal D2. These were within the range of values reported for H/C and O/C atomic ratios in literature for inertinite-rich coals (de la Rosa *et al*., 1992; Hanna *et al*., 1992; Mastalerz and Marc Bustin, 1993; Maroto-Valer *et al*., 1994). The H/C and O/C atomic ratios are major factors affecting the aromaticity *vis-à-vis* the extent of structural disorderliness in coals and chars (Lu *et al*., 2001). Both the H/C and O/C atomic ratios exhibited significant reductions in the transition from coals to chars. This can be attributed to the removal of the liptinites, aliphatics and lower molecular components of the coals during pyrolysis.

3.7.2 XRD Mineral Analyses

Minerals and or inorganic species present in both the coal and char samples was studied using the powder XRD technique and the Rietveld Autoquan quantification program. A summary of graphite (carbon) and of the total mineral content of the coal and char samples is presented in Table 3.9, while a detailed result of the mineral phase proportion expressed as a percentage of the total mineral content is given in Table 3.10. The idealised formulas of the mineral species (van Alphen, 2009; Web Mineral, 2009) are also included.

From Table 3.9 it can be observed that the total mineral phases reported for the coal samples from XRD analysis are higher than their respective ash content determined from proximate analysis. This is attributed to the ashing process of the proximate analysis at high temperature which may result to losses of some volatile mineral phases, despite the fact that the XRD technique measures the percentage of the

crystalline mineral matter only. A similar finding was made by Matjie, (2008). Total mineral phases of the chars are lower than their ash counterpart from proximate analysis. This is because the XRD technique does not account for the amorphous phases of the minerals and decompositions (van Alphen, 2009) may have occurred during the charring process.

Table 3.9: Percentage of graphite and total crystalline mineral phases of the coal and char samples from XRD results.

Sample ID	Graphite (carbon/ char)	Total mineral phases
Coal B	66.31	33.69
Char B	83.07	16.93
Coal C	66.53	33.47
Char C	83.72	16.28
Coal C2	63.96	36.04
Char C2	89.23	10.77
Coal D2	59.50	40.50
Char D2	87.56	12.44

Graphite (carbon) makes up the greater proportion of the coal and char samples from XRD mineral analysis. This further validates the results from both the proximate and ultimate analysis. The graphite content in the coal samples ranges from 59.5 *wt. %* for coal D2 to 66.5 *wt. %* for coal B.

The results from Table 3.10 show that all four coal samples are rich in the major coal minerals - kaolinite and quartz. Kaolinite content values (graphite free basis, (*gfb*)) ranges from 52.8 *wt. %, gfb* for coal D2 to 79.9 *wt. %, gfb* for coal C2, while quartz content values are between 6.19 *wt. %, gfb* for coal D2 and 17.6 *wt. %, gfb* for coal B. Other major mineral species dominant in the coal samples are calcite, dolomite gypsum and pyrite. Minor minerals observed in the coal samples include small amounts of muscovite and trace quantities of rutile and siderite. It can be observed that coal D2 has less of the clay minerals (kaolinite and quartz) and a very high proportion of gypsum (29.6 *wt. %, gfb*) relative to the other coal samples which may impart some catalytic effect during its utilisation.

Table 3.10: Mineral abundance of coals and chars (graphite free bases, (*wt. %, gfb*)).

Mineral Specie	**Idealised Chemical Formula**[1]	**Mineral Proportion** (*wt. %, gfb*)							
		Coal B	**Char B**	**Coal C**	**Char C**	**Coal C2**	**Char C2**	**Coal D2**	**Char D2**
Calcite	$CaCO_3$	4.03	-	4.31	0.61	2.52	4.00	2.52	1.93
Dolomite	$CaMg(CO_3)_2$	4.72	-	6.76	-	1.72	-	2.79	-
Gypsum	$CaSO_4 \cdot 2(H2O)$	4.86	-	7.66	-	1.08	-	29.6	-
Kaolinite	$Al_2[Si_2O_5](OH)_4$	55.5	-	55.6	-	79.9	-	52.8	-
Muscovite	$KAl_2(AlSi_3O_{10}(OH)_2)$	11.0	-	10.6	-	6.63	-	3.72	-
Pyrite	FeS_2	1.51	-	0.84	-	0.47	-	1.04	-
Quartz	SiO_2	17.6	32.2	13.1	37.4	6.38	19.9	6.19	33.2
Rutile	TiO_2	0.68	-	0.57	-	0.92	-	0.59	-
Siderite	$FeCO_3$	0.12	-	0.54	-	0.36	-	0.79	-
Cristobalite	SiO_2	-	20.1	-	24.0	-	38.9	-	25.1
Illite	$K_{1-1.5}Al_4[Si_{6.5-7}Al_{1-1.5}O_{20}](OH_4)$	-	14.2	-	7.13	-	8.91	-	2.33
Iron alpha	α-Fe	-	2.36	-	1.54	-	1.02	-	4.18
Microcline	$KAlSi_3O_8$	-	20.1	-	20.8	-	22.6	-	18.2
Oldhamite	$Ca_{0.9}Mg_{0.05}Fe_{0.05}S$	-	8.62	-	5.96	-	3.06	-	10.3
Sodalite	$Na_8Al_6Si_6O_{24}Cl_2$	-	1.24	-	1.47	-	1.30	-	2.65
Troilite	FeS	-	1.18	-	1.11	-	0.28	-	2.10
Total		**100.02**	**100.00**	**99.98**	**100.02**	**99.98**	**99.97**	**100.04**	**99.99**

[1]- van Alphen (2009); Web Mineral Data (2009)

As seen in Tables 3.9 and 3.10, the transition from parent coals to chars via the charring process caused some loss (water of crystallisation), decomposition and or transformation of the mineral species in the parent coal as it changed to char at 900 °*C*. Graphite percentage contents increased from parent coal to char in all four samples ranging in value from 83.07 *wt. %* for char B to 89.23 *wt. %* for char C2 up from 59.5 and 66.53 *wt. %* respectively for the parent coals. This is as expected since the devolatilisation of the coal results in the enrichment of the resulting char in carbon and ash as seen in the proximate and ultimate analyses results of the samples (Table 3.8).

On graphite free basis, quartz mineral (SiO_2) increased by a factor of > 2 in the transition which was more significant in chars D2 and C2. Quartz in Char D2 increased significantly from 6.19 *wt. %, gfb* in the parent coal to 33.2 *wt. %, gfb*. The same trend was observed for char C2 with a quartz content of 19.9 *wt. %, gfb* up from 6.38 *wt. %, gfb* value of the precursor coal. This may be attributed to the transformation of kaolinite and muscovite in the parent coal.

Calcite was not observed in char B and only very little (0.61 - 4.0 *wt. %, gfb*) was observed in the other chars. Calcite and quartz were the only mineral species that were present in both the parent coals and the chars (except char B). The clay minerals (illite and microline) and silicates (quartz and cristobalite) were the most abundant minerals in the chars. Pyrite was reduced to alpha iron and some interactions with siderite in the parent coal yielded troilite in the chars. Other mineral species in the chars are oldhamite and traces of sodalite.

3.7.3 Ash Analysis (XRF)

The normalised proportions (Loss on Ignition (*LOI*) and sulphur free basis) of major inorganic composition of the char ashes from the XRF spectroscopy analysis are presented in Table 3.11.

Considering the *LOI* and the total ash content, it can be seen that the ash content from proximate analysis corresponds well with the total ash content from XRF result. This is due to the similarity of the ashing process of the two techniques at high temperature

(815 *℃*). The XRF technique used is regarded as only semi-quantitative for sulphur (Matjie, 2008; Loubser and Verryn, 2008), hence the sulphur contents were not reported. From the result, SiO_2 and Al_2O_3 are the most abundant chemical components in the ash of the chars which compares well with the XRD mineral analysis results. These are derived from the clay minerals (quartz and kaolinite) that form the bulk of the mineral in coal and subsequent chars (Spears, 2000).

The presence of Fe_2O_3 in al the char samples can be attributed to the pyrite and siderite in the original coal as well as to the troilite and iron alpha detected in the chars. CaO and MgO were also detected in all of the four char samples which is a reflection of the dolomite and calcite phases in the parent coal samples and oldhamite in some appreciable quantities in the chars, with a larger contribution to CaO content of char B suspected to be due to the high content of gypsum in the parent coal B. The lowest value of CaO content was observed in char C2 at 3.02 *wt. %, lfb*.

Table 3.11: Char sample ash chemistry on *LOI* and sulphur free basis (*wt. %, lfb and sfb*).

Sample ID	**Mineral Species** (*wt. %, lfb and sfb*)			
	Char B	**Char C**	**Char C2**	**Char D2**
SiO_2	50.9	49.9	50.8	46.9
Al_2O_3	29.4	31.7	39.7	34.5
Fe_2O_3	5.03	3.59	2.50	4.75
CaO	8.78	8.16	3.02	8.18
MgO	1.90	2.16	0.68	2.30
MnO	0.06	0.05	0.03	0.08
TiO_2	1.68	1.91	2.38	2.29
Na_2O	0.23	0.23	0.26	0.14
K_2O	0.74	0.98	0.37	0.48
P_2O_5	1.18	1.31	0.23	0.33
Cr_2O_3	0.09	0.04	0.05	0.04
Total (*wt. %, lfb*)	**99.99**	**100.03**	**100.01**	**99.99**
LOI (*wt. %, adb*)	71.3	67.5	68.9	67.3
Ash content of chars (*wt. %, adb*)	28.5	33.2	34.0	36.8
Alkali Index (-)	**5.92**	**6.15**	**2.55**	**7.17**

It is should be noted that this analysis was confined to the chars only as the motivation for the analysis was to study the inherent catalytic influence, if any, of the high ash components of the chars on their CO_2 reactivity and the parent coals were not used for the reactivity experiments.

The presence of K_2O in all the chars, with the highest value in char C, is related to the muscovite in the parent coals and to the illite and microcline in the chars, while Na_2O and TiO_2 are derived from the sodalite in the chars and rutile in the parent coals respectively.

A significant contribution of this analysis is the study of the catalytic effects due to the presence of these elemental components by determining the respective lumped parameter, alkali index *AI*, of the chars which are presented in Table 3.11. Walker and Hippo (1975), Miura *et al*. (1989), Hüttinger and Natterman (1994), Tomita (2001), Zhang *et al*. (2006), and Lee (2007) have all reported that elemental components, such as Fe_2O_3, CaO, MgO, Na_2O, K_2O, impart a catalytic effect on the gasification reaction of coals and chars. The *AI*, refers to the ratio of the total weight fraction of the basic species in the ash (CaO, MgO, K_2O, Na_2O and Fe_2O_3) to the total weight fraction of the acidic compounds (SiO_2 and Al_2O_3) in the ash, multiplied by the ash contents in weight percent of the chars. This formulation is shown as Equation 3.12; while the *AI* results of the chars are presented in Table 3.11.

$$AI = \left(\frac{CaO + MgO + K_2O + Na_2O + Fe_2O_3}{SiO_2 + Al_2O_3} \right) \times ash\% \qquad (3.12)$$

3.7.4 X-ray Diffraction (XRD) Carbon Crystallite Analysis

The second aspect of analysis involving the use of the X-ray diffraction technique was the study of the carbon crystallite properties of the coal and char samples. To reduce noise and the effects of mineral matter on the XRD diffractogram and for a simplified study of the carbon fraction, a three stage HCl-HF-HCl demineralisation was conducted on the samples. The outcome of this, presented as proximate analysis of the samples together with the effectiveness of the process, is summarised in Table 3.12.

Table 3.12: Proximate analysis of raw and demineralised coal and char samples (*wt. %, db*).

Sample ID		VM (*wt. %, db*)	Ash (*wt. %, db*)	Fixed Carbon (*wt. %, db*)	E_d [1] (%)
Coal B	Raw	24.3	26.6	49.0	96.7
	Demin[2]	27.0	0.88	72.2	
Char B	Raw	1.21	28.8	70.0	89.1
	Demin	5.79	3.13	91.1	
Coal C	Raw	22.1	30.7	47.1	97.9
	Demin	25.3	0.66	74.0	
Char C	Raw	0.81	33.6	65.6	93.9
	Demin	5.59	2.06	92.4	
Coal C2	Raw	18.9	29.7	51.3	98.3
	Demin	20.3	0.5.0	79.2	
Char C2	Raw	3.25	34.5	62.2	89.8
	Demin	5.49	3.52	91.0	
Coal D2	Raw	22.4	28.8	48.7	96.7
	Demin	27.2	0.94	71.8	
Char D2	Raw	2.71	36.8	60.5	90.5
	Demin	5.55	3.48	91.0	

[1]- E_d – Effectiveness of demineralisation [2]- Demineralised sample

It is obvious from the result that more effective demineralisation was achieved on the parent coals (96.7- 98.3%) than on the chars (89.1- 93.9%) with the corresponding ash contents reduced to 0.5 - 0.94 *wt. %, db* and 2.06 - 3.52 *wt. %, db* respectively. This is to be expected since the pyrolysis reaction at 900 °*C* that leads to the chars, drives off the volatiles and hardens the chars. This may prevent the demineralisation agent from easily reaching the mineral inclusions. This will also culminate in an increase in both the skeletal and bulk density of the resulting chars. An increase in both the fixed carbon and volatile matter content was also observed for the demineralised coal and char samples. Similar results were reported by Lu *et al.* (2001), Maity and Mukherjee (2006), Kawakami *et al*. (2006), and Van Niekerk (2008).

The raw diffractograms from the XRD analysis for the demineralised coal and char samples, corrected for polarisation and geometrical factors, are shown in Figure 3.2. The background due to the amorphous carbon fraction was further removed and the diffractograms smoothened with the HighScore Plus peak analysis tool and are presented in Figure 3.3. The diffractograms of all the demineralised coal and char samples investigated in this study possess the same graphitic features as those reported in literature (Franklin, 1950 and 1951; Hirsch, 1954; Alexander and Sommer, 1959; Shiraishi and Kobayashi, 1973; Kumar and Gupta, 1995; Lu *et al*., 2001, 2002a and 2002b; Aso *et al*., 2004; Kawakami *et al*., 2006; Maity and Mukherjee, 2006; Wu *et al*., 2008).

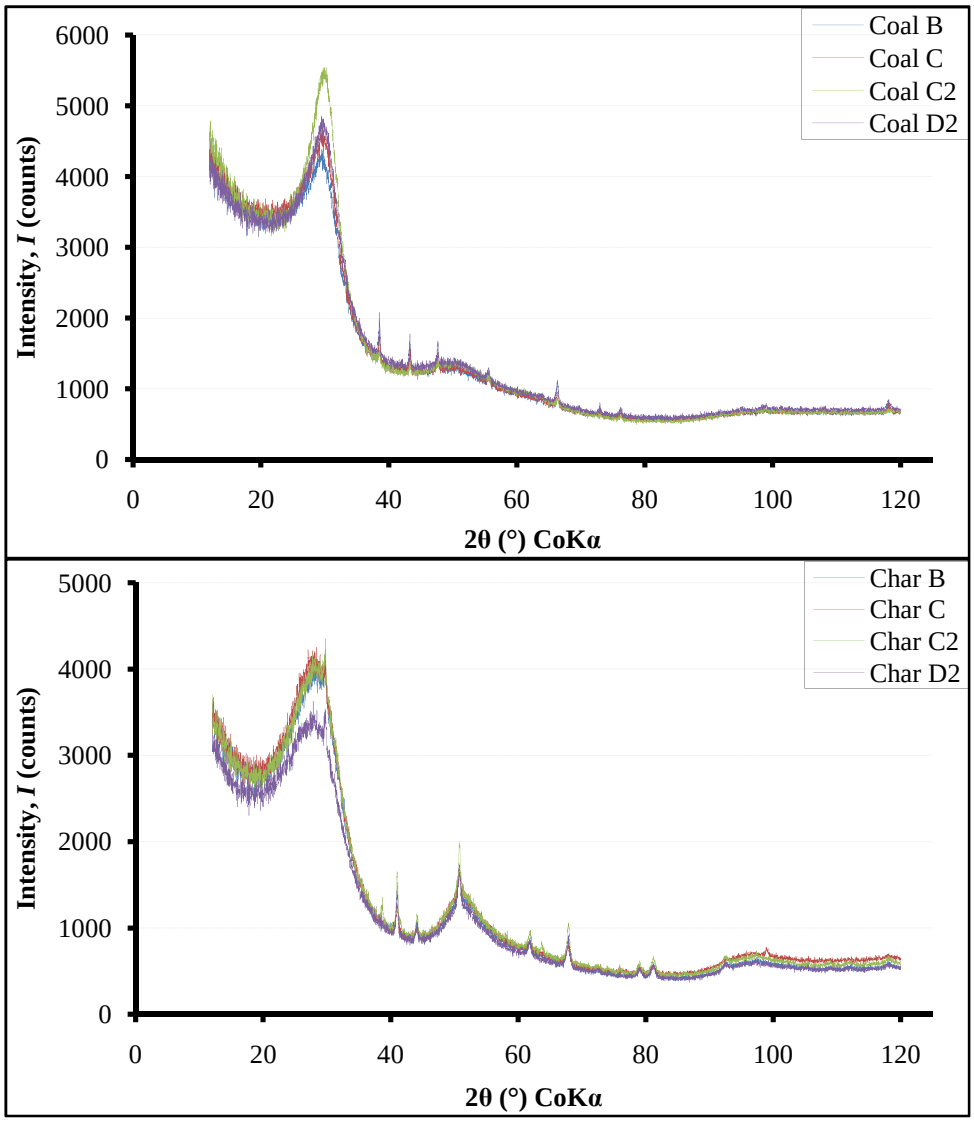

Figure 3.2: Raw diffractograms of coal and char samples.

The graphitic features were established by the presence of the (*002*) band corresponding to the (*00l*) position of graphite. The (*00l*) position is related to the inter-layer spacing of graphite and its resemblances in the diffractograms ((*002*) band) occur at 29.56° ≥ 2θ ≤ 30.05° for the coals; and 28.66° ≥ 2θ ≤ 29.71° for the chars. The (*10*) and (*11*) bands that correspond to the (*hk0*) lines of graphite, related to the hexagonal ring structure, were also observed. The (*10*) bands occur at position 50.90° ≥ 2θ ≤ 51.60° and 51.90° ≥ 2θ ≤ 52.90°, while the (*11*) band was observed at 98.21° ≥ 2θ ≤ 98.59° and 96.70° ≥ 2θ ≤ 97.45° for the coals and chars respectively. These peak positions are significant in the calculation of the crystallite lattice parameters.

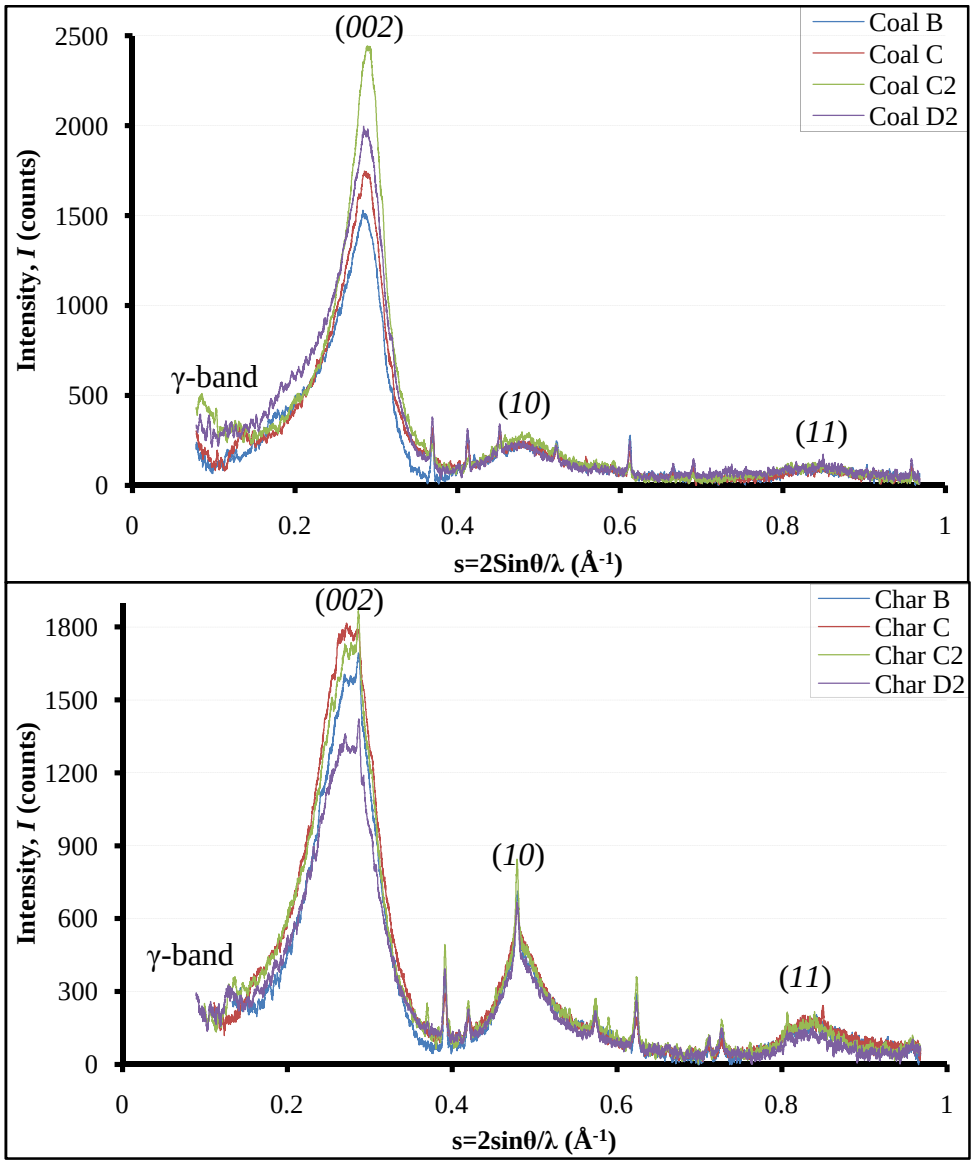

Figure 3.3: Corrected and smoothened diffractograms of coal and char samples.

The assymetry exhibited by the (*002*) band necessitated the dilineation of the peak into the d_{002} peak and the γ-side band which appears as a shoulder band in the difractograms (Franklin, 1950 and 1951; Hirsch, 1954; Ergun and Tiensuu; 1959; Schoening, 1983; Lu *et al*., 2001; Lu *et al*., 2002a). The former is associated with the aromatic ring stacking while the later is due to the aliphatic side chains. The small spikes on the diffractogram are peaks of traces of minerals still remaining in the demineralised samples as indicated by the effectiveness of demineralisation, E_d, (Table 3.12).

The inter-layer spacing was calculated from the (*002*) peak position using the Braggs equation, while the crystallite height, L_c, and diameter, L_a, were determined from the peak positions, and the full width at half maximum (FWHM) of the (*002*) and (*10*) peaks respectively. The (*11*) band was not used due to its diffuse and obscure nature which makes quantitative analysis difficult.

The characteristics of the diffractograms and the annealing effects of the transition from parent coal to char at 900 *℃* (samples B and C) are expounded in Figure 3.4. The (*002*), (*10*) and (*11*) peaks of the chars are broader than those of the precursor coals, while the γ-shoulder-band is more prominent in the coals than in the chars. The broadening of the (*002*) peak in the diffractograms obtained for the chars is due to the closer packing and structural re-ordering, re-orientation and better alignment of the aromatic carbon layers, which results in an increase in the inter-layer spacing and a decrease in both the crystallite height and diameter of the chars relative to the original coals. The broadening of peaks is evidence of a decrease in carbon crystallite size, while sharper peaks are signs of growth of the carbon crystallite (Kuroda and Akamatu, 1959; Short and Walker, 1963; Kumar and Gupta, 1995; Lu *et al*., 2002a and 2002b; Wu *et al*., 2008).

Crystallite condensation, as observed in this study, was also observed by Takagi *et al*. (2004) for chars produced at 760 *℃* and 900 *℃*. A careful analysis of the scatter of the results reported by Kawakami *et al*. (2006), also shows an increase in inter-layer spacing between chars prepared at 900 *℃* and 1200 *℃*. It should be noted that significant crystallite growth usually starts from 1600 *℃* (Kuroda and Akamatu, 1959; Kumar and Gupta, 1995; Lu *et al*. 2002a and 2002b; Wu *et al*. 2008), with the

experiments conducted by these investigators, confined to temperatures above 1200 ℃. Takagi *et al*. (2004) however noted that broadening of peaks at lower temperatures of heat treatment (350 - 920 ℃) is more significant for lower rank coals, while for higher rank coals, sharper peaks may be observed.

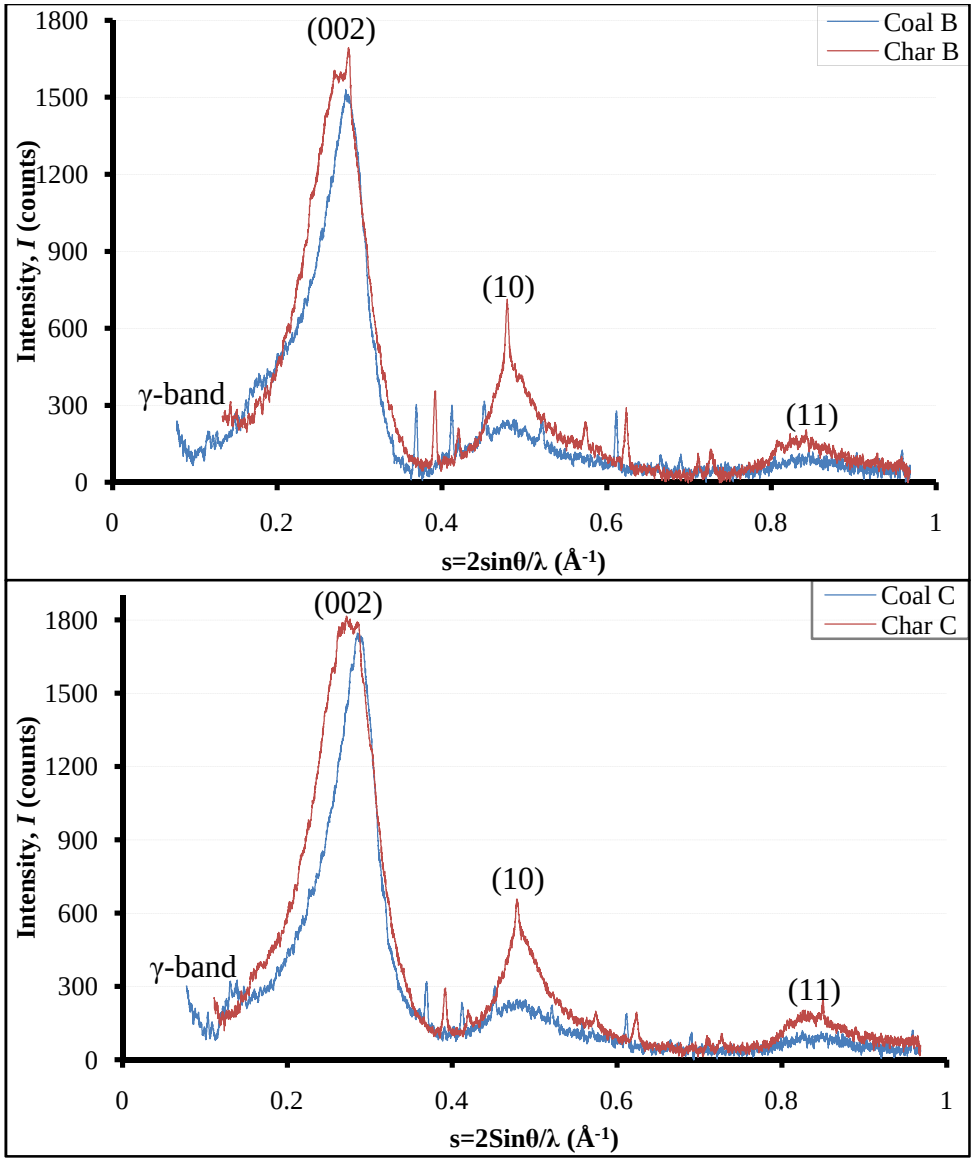

Figure 3.4: Comparison of coal and char diffractograms for samples B and C.

The diffuse and in some cases almost absent γ-sideband in the diffractograms of the chars is due to the loss of the aliphatic side chain during the char production process. This culminates in a more ordered structure (Russell *et al*. 1999; Davis *et al*. 1995; Lu *et al*. 2001; Van Niekerk, 2008), which impacts on the chemical properties of the

char, as aromaticity and the fraction of amorphous carbon and other crystallite parameters.

Van Niekerk (2008), however, reported a contrasting result for the investigated inertinite-rich Highveld coal sample, as a prominent γ-side band was observed, which was entirely missing in the diffractogram of the vitrinite-rich Waterberg coal. This means that the vitrinite-rich coal is structurally more ordered than the inertinite-rich sample. The result contradicts the high aliphatic content of vitrinite-rich coals (Choi *et al*., 1989; dela Rosa *et al*., 1992) and may have led to his inability to determine the aromaticity of the studied vitrinite-rich coal sample using XRD technique.

3.7.4.1 Determination of Aromaticity of Coal and Char Samples

The aromaticity of both coal and char samples were determined from the areas under the (*002*) peak and the γ-side band (Lu *et al*., 2001, 2002a and 2002b; Maity and Mukherjee, 2006). This was done using a curve fitting analysis tool on the HighScore Plus application. A confirmation was conducted on the result using the peak analysis, curve fitting and the data analysis tool of Origin 6.1 to determine the areas under the (*002*) peak and the γ-side band. The curve fitting and analysis of the two peaks to get the respective peak areas for coal B and Char C2, using HighScore Plus, is shown in Figure 3.5.

A comparison of the results from the two methods described above is summarised in Table 3.13. It can be seen from the table that the results obtained from the two different data analysis applications are very similar to each other, thus validating the results.

Table 3.13: Comparison of aromaticity results from HighScore Plus and Origin 6.1.

Determination of Aromaticity (fractional values (-))								
	Coal B	**Char B**	**Coal C**	**Char C**	**Coal C2**	**Char C2**	**Coal D2**	**Char D2**
By HighScore Plus	0.7993	0.8822	0.8106	0.9091	0.8527	0.9513	0.7539	0.8489
By Origin 6.1	0.8011	0.8839	0.8113	0.9192	0.8517	0.9483	0.7513	0.8470

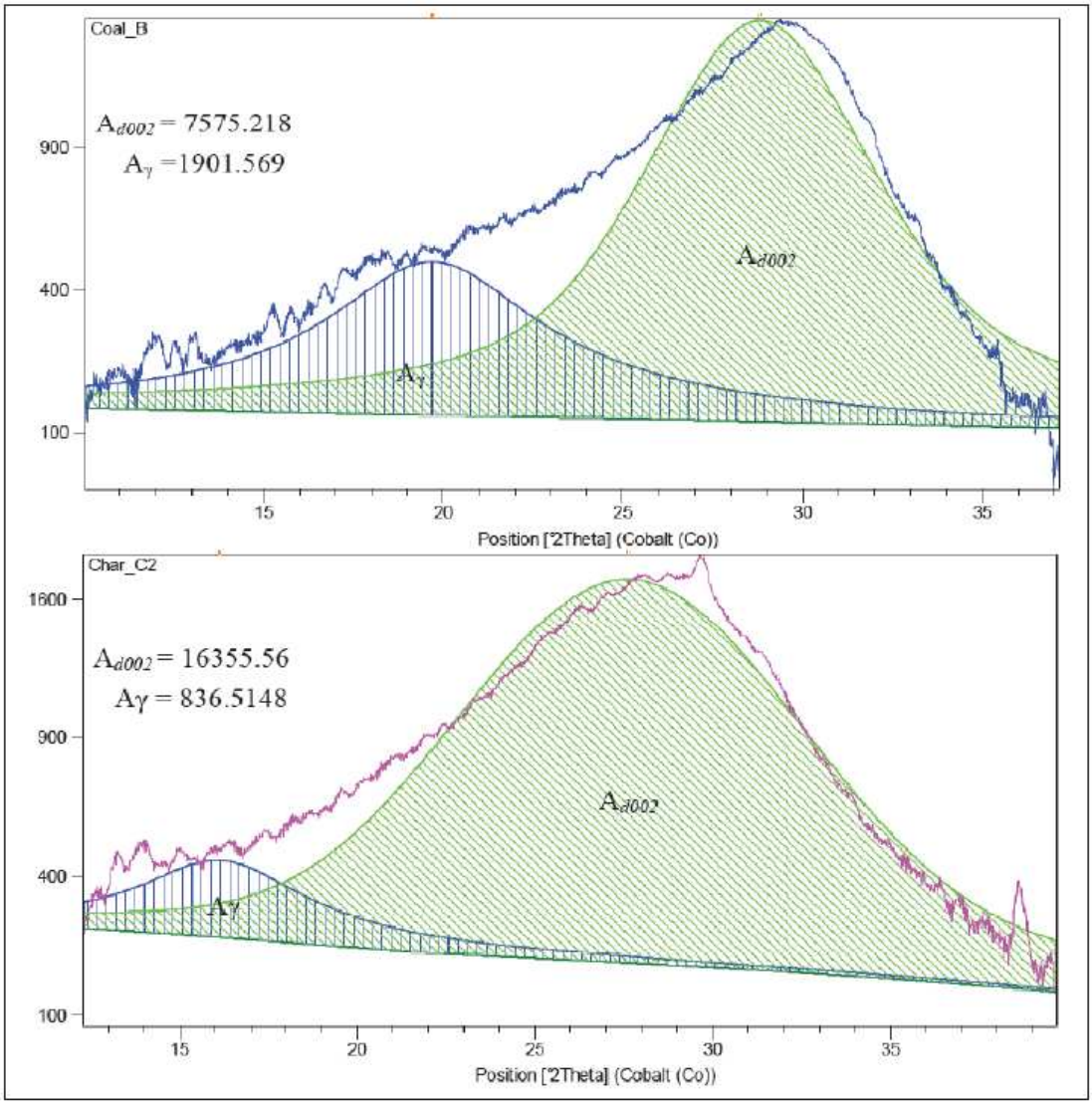

Figure 3.5: Determination of area under d_{002} and γ- band using HighScore Plus for coal B and char C2.

3.7.4.2 Determination of Fraction of Amorphous Carbon of the Coal and Char Samples

The determination of the fraction of amorphous carbon contained in both the coal and char samples was carried out by normalising the diffractograms shown in Figure 3.4 to obtain the reduced intensity curve of the (*002*) peak (Figure 3.6), according to the method proposed by Franklin (1950) and variously used by Ergun and Tiensuu (1959); Short and Walker (1963); Lu *et al*. (2001, 2002a, and 2002b); Kawakami *et al*. (2006).

The symmetrical section of the (*002*) band used for this analysis for coal C2 and char C is shown in Figure 3.6. In Table 3.14, the I_{max}, S_{max}, and other parameters for the calculation of the fraction of amorphous carbon in coal C2 and char C are presented. It should be noted first, that the results of X_A, are returned as negative and reported as absolute values, and second, that the reciprocal of S_{max} should be equal to the inter-layer spacing, d_{002}, if the (*002*) band symmetric profile is correct.

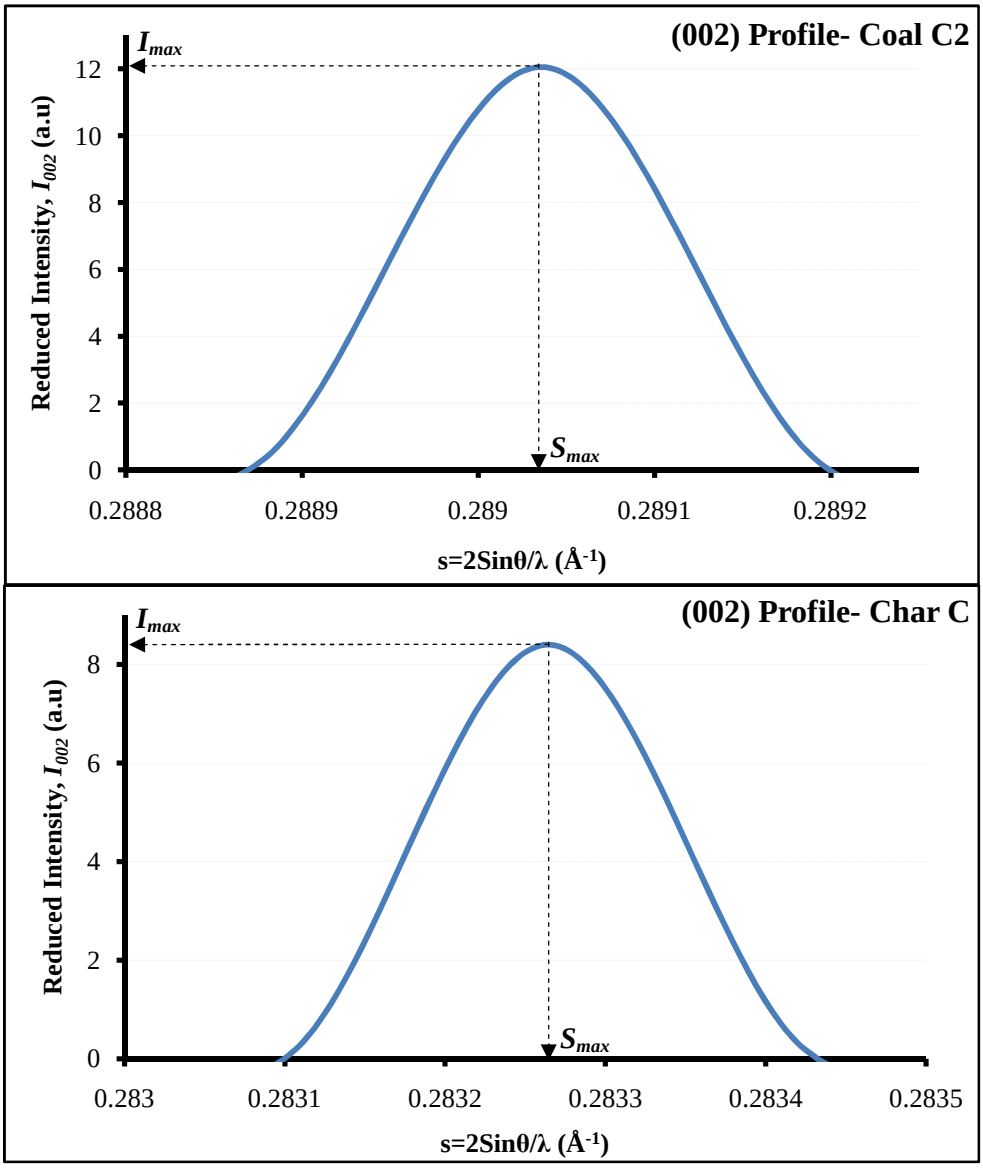

Figure 3.6: Determination of amorphous fraction of carbon, X_A, from (*002*) profile of coal C2 and char C.

Table 3.14: Determination of amorphous fraction of carbon for coal C2 and char C.

Sample ID	**Coal C2**	**Char C**
I_{max}	12.06	8.405
d_{002}	3.460	3.530
N_{ave}	5.900	5.410
S_{max}	0.289	0.283
$I\text{-}X_A/1\text{-}X_A$	7.860	6.960
X_A	0.613	0.242

Results from the carbon fraction analysis, using XRD techniques, are summarised in Table 3.15.

Table 3.15: Result on carbon crystallite analysis using XRD.

Sample ID	**Coal B**	**Char B**	**Coal C**	**Char C**	**Coal C2**	**Char C2**	**Coal D2**	**Char D2**
d_{002} (Å)	3.49	3.58	3.48	3.53	3.46	3.49	3.46	3.50
L_c (Å)	15.5	10.5	15.4	11.4	16.9	11.4	14.8	11.9
N_{ave} (-)	5.45	3.92	5.41	4.23	5.90	4.26	5.28	4.40
L_a (Å)	9.32	7.52	12.2	10.1	12.6	11.2	12.0	10.7
f_a (-)	0.80	0.88	0.81	0.92	0.85	0.95	0.75	0.85
X_A (-)	0.49	0.28	0.51	0.24	0.61	0.23	0.66	0.48
DOI[1] (-)	0.59	0.37	0.60	0.30	0.67	0.27	0.75	0.56

[1]- Degree of disorder index

It can be observed from the results, that apart from the inter-layer spacing, d_{002}, and aromaticity, f_a, which generally increased from coal to char, the other parameters (the average crystallite diameter, L_a; the average crystallite height, L_c; the average number of aromatic layers per carbon crystallite, N_{ave}; the fraction of amorphous carbon, X_A; and the degree of disorder index, *DOI*) all generally decreased from parent coals to chars.

The increase in the inter-layer spacing from parent coal to char is as a result of the loss of moisture and volatiles and of the annealing of the carbon crystallites that causes the disordered carbons of the coal to be more structurally ordered and orientated in the chars. The decrease in lattice parameters (L_c, L_a, and N_{ave}) is as a result of a more compact, ordered and orientated structure imparted to the char by the heat treatment process (Davis *et al*., 1995; Russell *et al*., 1999). This hardens the char and influences both its skeletal and bulk density. Similar findings were made by Short and Walker (1963); Takagi *et al*. (2004); Kawakami *et al*. (2006); Bouhadda, *et al*. (2007) and Wu *et al*. (2008).

It is generally known that the inter-layer spacing increases with elemental carbon content *vis-à-vis* coal rank (Lu *et al*., 2001; Takagi *et al*., 2004; Maity and Mukherjee, 2006). This was not observed on the coal samples and thus not reported, and may be attributed to the fact that all four coal samples are about the same rank. Coal B, C, and C2 are bituminous medium rank C with the same elemental carbon content of 73.1 *wt. %, daf*; while coal D2 is classified as bituminous medium rank D with elemental carbon content of 68.1 *wt. %, daf*.

The dependency of aromaticity on the atomic hydrogen-carbon ratio is presented in Figure 3.7(i) and follows an almost linear trend of decreasing aromaticity with increasing hydrogen-carbon ratio. This can be explained by the fact that hydrogen content in coal is associated with the low molecular mass and aliphatic group and an increase in the proportion of this group will result in a higher volatile matter content and lower aromaticity (Choi *et al*., 1989). Similar trends were reported by Solum *et al*. (1989), Maroto-Valer *et al*. (1994), and are validated by the result of Lu *et al*. (2001). The correlation of the fraction of amorphous carbon in the coal samples to the atomic hydrogen-carbon ratios yielded a wide scatter (not reported) but increased with the oxygen-carbon ratios (Figure 3.7 (ii)). The plot of aromaticity versus the atomic oxygen carbon ratio exhibited a wide scatter and was not reported as well.

It may thus be concluded that while aromaticity of coals depend on the atomic hydrogen ratio, the fraction of amorphous carbon may be influenced appreciably by the atomic oxygen-carbon ratio which needs to be investigated further. However, most investigators have noted that the mechanism of structural ordering is not well understood (Franklin, 1951; Hirsch, 1954; Kumar and Gupta, 1995; Lu *et al*., 2001).

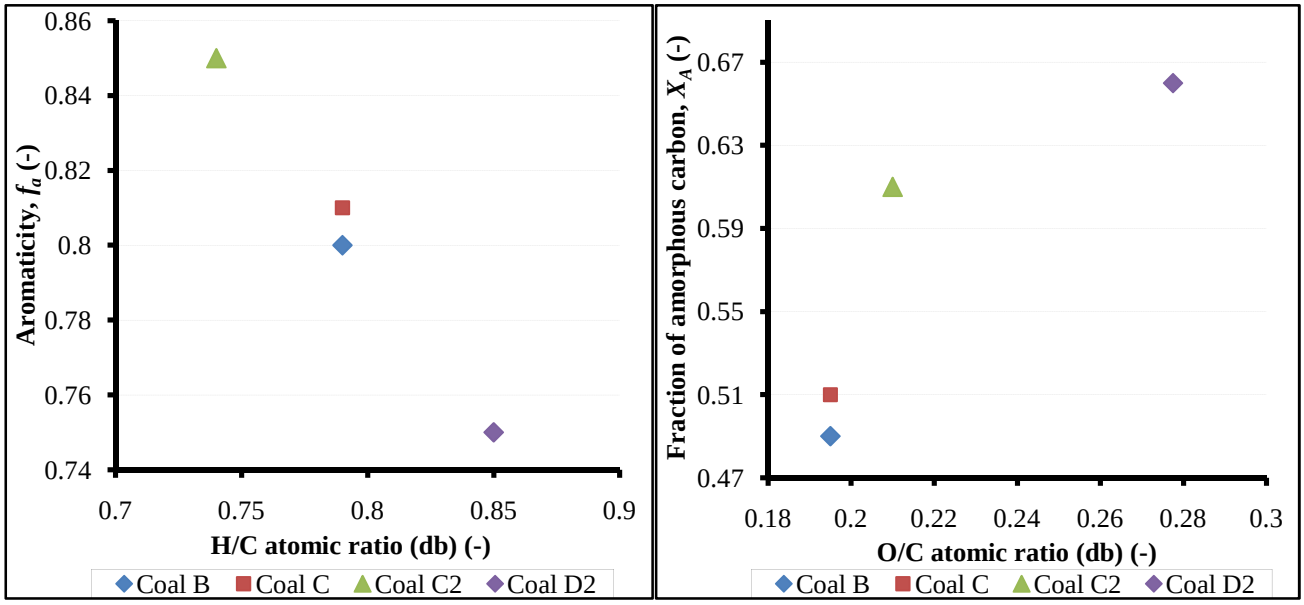

(i) Relationship between aromaticity and hydrogen-carbon ratio of coals

(ii) Relationship between fraction of amorphous carbon and oxygen-carbon ratio of coals

Figure 3.7: Relationship between aromaticity and fraction of amorphous carbon and the atomic ratios of hydrogen and oxygen to carbon in coal samples.

The increase in aromaticity from coals to chars is related to the loss of aliphatic side chains in the parent coal (evident from the obscurity and near-loss of the γ-sideband as observed in the diffractograms of the chars) due to the charring process. Since the fraction of amorphous carbon refers quantitatively to the fraction of disordered carbon, it should be expected that its content decrease from the parent coal to the annealed chars, the structure of which is more ordered due to the annealing of the turbostratic structure of the parent coals and to the formation of a more crystalline structure in the chars. The results of Senneca *et al*. (1998); Lu *et al*. (2001, 2002a, and 2002b); Kawakami *et al*. (2006); and Maity and Mukherjee (2006) correlate well with the outcome of this study.

The decrease of the degree of disorder index (*DOI*) from coal to char is an indication that the chars are more ordered and more crystalline than the parent coal. This was corroborated by the increase in the aromaticity, and the decrease in the average crystallite height and diameter, a further indication of the compactness and the degree of orderliness of the chars (Lu *et al*., 2002a).

Correlations were made of some of the carbon crystallite parameters of the chars, as shown in Figure 3.8. Both the fraction of amorphous carbon and the degree of disorder index was found to decrease with increasing aromaticity (Figure 3.8(i) and (ii)). Increasing aromaticity is an indication of increasing structural orderliness, hence a decreasing *DOI* and fraction of amorphous carbons (Davis *et al.*, 1995; Maity and Mukherjee, 2006; Lu *et al.*, 2002a; Wu *et al.*, 2008).

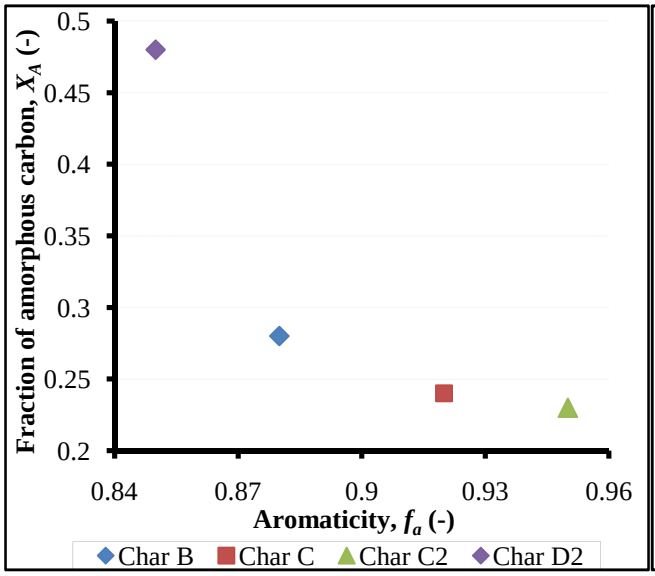

(i) Relationship between aromaticity and fraction amorphous carbon in chars

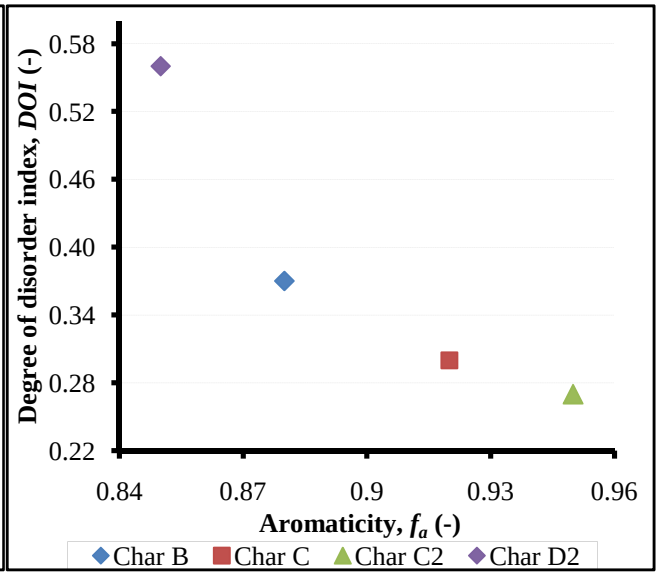

(ii) Relationship between aromaticity and degree of disorder index (*DOI*) in chars

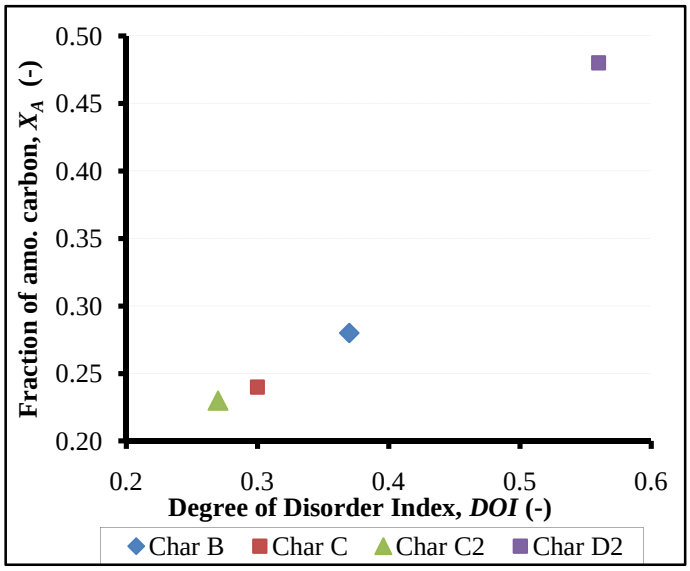

(iii) Relationship between fraction of amorphous carbon and degree of disorder index of chars

Figure 3.8: Relationship between various crystallite parameters of char samples.

The fraction of amorphous carbon was found to increase with degree of disorder index (*DOI*) (Figure 3.8(iii)). This is not unusual as an increase in both parameters is indicative of a higher relative abundance of disordered carbon (Lu *et al*., 2002a)

Although not reported because char D2 was out of trend, the aromaticity (considering chars B, C and C2) was observed to decrease with an increase in both the inter-layer spacing and fraction of amorphous carbon. This is to be expected, given the fact that as d_{002} increases further away from the inter-layer spacing of graphite (3.35 - 3.44 Å) (Franklin, 1951, Hirsch, 1954, Ergun, 1968, Kumar and Gupta, 1995; Takagi *et al*., 2004), the disorder and non-alignment of the carbon structure increases. It is also expected that the fraction of amorphous carbon will correspondingly increase with increasing inter-layer spacing – an indication of the level of structural ordering and the amount of aromatic carbons.

3.7.5 Petrographic Analyses

Results and discussions relating to the petrographic analysis of the coal and char samples are presented in this section. Results presented include the reflectance properties of both vitrinite- and total maceral- reflectance scans and organic component analysis which include maceral, microlithotype, carbominerite and char form analysis. Results from minerite analysis which describes the inorganic components of the samples under the petrographic microscope and general condition analysis are also presented.

3.7.5.1 Reflectance Properties

Reflectance analysis has been distinguished as a vital tool in determining the rank of coal using the rank parameter based on vitrinite random reflectance (Cameron and Hunt, 1985; Falcon and Snyman, 1986; Snyman, 1989; Cloke and Lester, 1994). For this study, the coal vitrinite maceral, collotelinite was used as the reference material as its reflectance increases uniformly as the coalification process progresses and is independent of the vitrinite content and coal grade (Falcon and Snyman, 1986; du Cann, 2007). Reflectance measurements were conducted in oil immersion in

accordance with ISO 7404 - 5 (1994). A summary of the major reflectance properties of the coal and char samples is shown in Table 3.16.

The vitrinite random reflectance results showed that according to the ISO-11760 (2005) classification of coals, three of the coal samples: coal B, C and C2 were characterised as Bituminous Medium Rank C (0.65 - 0.78 *Rr%*); while coal D2 was classified as Bituminous Medium Rank D (0.56 - 0.58 *Rr%*) (du Cann, 2007).

The mean vitrinite random reflectance values of the char samples are 0.67, 0.72, 0.75 and 0.56 *Rr%* respectively for coals B, C, C2 and D2. Vitrinite class distribution ranges from V5 - V9 for both coals B and C and V4 - V12 and V4 - V7 for coal C2 and D2 respectively with a standard deviation of < 0.1. This is an indication that, with the exception of coal C2, whose vitrinite-class distribution was similar to that of a blend coal with standard deviation of 0.129, the parent coals are single seam, non-blend coals (terminology of the ECE-UN International codification System for Medium and High Rank Coals). Only coal C2, which exhibited a slightly extended vitrinite-class distribution (du Cann, 2007), was observed to have some abnormalities possibly caused by in situ thermal effects. Similar findings were made by Kaitano (2007) and Everson *et al*. (2008b).

The vitrinite random reflectance scan histograms of the coal samples are presented in Appendix A. This property was not determined for chars due to significant changes imparted to the coal vitrinite during the charring process at 900 *°C*. Kaitano (2007) and Phiri (2010) reported comparable observations on their investigated chars.

The total maceral reflectance scan analysis was also conducted on the coal and char samples. This involved taking 250 readings on all organic components (vitrinites, liptinites and inertinites) and the results obtained are summarised in Table 3.16. The overall assessment of the general reflectivity of the macerals shows that the carbon-rich char has attained higher varying levels of reflectance. Thus, very significant shifts were displayed in the mean random reflectance (*Rsc%*) values of the chars (varying up to 5.3 *Rsc%*) compared to the original coals (varying up to 1.6 *Rsc%*). Increasing reflectance of the chars indicates: decreasing volatiles; increasing carbon content; increasing molecular ordering; and a corresponding increase in ignition temperature and burn-out time (Kaitano, 2007; du Cann, 2008; Everson *et al*., 2008b).

Table 3.16: Reflectance properties of coal and char samples.

Sample ID	**Coal B**	**Char B**	**Coal C**	**Char C**	**Coal C2**	**Char C2**	**Coal D2**	**Char D2**
Vitrinite Random Reflectance Scan								
Mean vitrinite random reflectance, Rr (%)	0.67	-	0.72	-	0.75	-	0.56	-
Range of readings	0.4 - 0.8	-	0.5 - 0.9	-	0.4 - 1.2	-	0.4 - 0.7	-
Standard deviation, σ (%)	0.082	-	0.092	-	0.129	-	0.062	-
Vitrinite-class distribution	V5 - V9	-	V5 - V9	-	V4 - V12	-	V4 - V7	-
Rank of coal	Bit. Med. Rank C	-	Bit. Med. Rank C	-	Bit. Med. Rank C	-	Bit. Med. Rank D	-
Total Maceral Reflectance Scan								
Mean random reflectance of scan, *Rsc*, (%)	1.27	5.28	1.30	5.19	1.63	4.43	1.15	5.07
Range of readings	0.10 - 2.8	3.7 - 6.8	0.10 - 2.6	3.4 -6.5	0.10 - 2.6	1.7 - 6.4	0.10 - 2.3	1.7 - 6.3
Standard deviation, σ (%)	0.542	0.588	0.492	0.596	0.382	1.127	0.458	0.715

These have profound effects on the performance of the various carbon conversion processes (Falcon and Snyman, 1986; Snyman, 1989; Cloke and Lester, 1994; du Cann, 2007). The total maceral reflectance scan histograms for the coal and char samples are included in Appendix A and were found to agree very well with the results of Kaitano (2007), Everson *et al*. (2008b) and Phiri (2010) on their various studies of chars derived from inertinite-rich, high ash, South African low grade coals.

3.7.5.2 Maceral Analysis of Parent Coals

The analyses of the macerals or organic compositions and visible minerals of the parent coals were conducted by point-count technique and results reported as volume percent on a mineral matter basis according to ISO 7404 - 3 (1994). A summary of this analysis including the inertinite-vitrinite ratio of the coal samples is given in Table 3.17, while the detailed results are presented in Table 3.18. All four coal samples were characterised as inertinite-rich with total inertinite content ranging from 54 *vol. %, mmb* for coal B to 79 *vol. %, mmb* for coal C2. The total vitrinite content was observed to be low in the samples, with coal B having the highest values of 28 *vol. %, mmb* and coal C2, a very low value of 3 *vol. %, mmb*. Liptinite content of the coals was also observed to be very low; < 4 *vol. %, mmb* in all the samples.

The ratio of inertinite to vitrinite macerals of the parent coals (on mineral matter basis) are: 1.93; 3.00; 26.3 and 4.70 respectively for coals B, C, C2 and D2.

Table 3.17: Maceral component summary of the coal samples (*vol. %, mmb*).

Sample ID	**Coal B**	**Coal C**	**Coal C2**	**Coal D2**
Vitrinite	28	19	3.0	13
Liptinite	3.0	3.0	3.0	4.0
Inertinite	54	57	79	61
Inertinite-vitrinite ratio	1.93	3.00	26.3	4.70

Table 3.18: Maceral compositions of coal samples (*vol. %, mmb*).

Coal ID	Vitrinite (*vol. %,mmb*)			Liptinite (*vol. %,mmb*)			Inertinite (*vol. %,mmb*)							(*vol. %,mmb*)	
	VIT	PV	TV	S/R/C	ALG	TL	RSF	ISF	F/ SEC	MIC	R INT	I INT	TI	Visible Minerals	Total Reactives
B	27	1	28	3	0	3	7	13	3	1	6	24	54	15	44
C	19	0	19	3	0	3	7	13	3	1	9	24	57	21	38
C2	3	0	3	3	0	3	14	17	4	2	14	28	79	15	34
D2	13	0	13	4	0	4	10	19	4	1	8	19	61	22	35

NOMENCLATURE:

VIT : Vitrinite

PV : Pseudo-vitrinite

TV : Total vitrinite

S/R/C : Sporinite / Resinite / Cutinite

ALG : Alginite

TL : Total liptinite

RSF : Reactive semifusinite

ISF : Inert semifusinite

F/SEC : Fusinite / Secretinite

MIC : Micrinite

R INT : Reactive Inertodetrinite

I INT : Inert Inertodetrinite

TI : Total inertinite

Total reactives = TV+TL+RSF+RINT

On a maceral component basis, pure vitrinite (3 - 27 *vol. %, mmb*), inert semifusinite (13 - 19 *vol. %, mmb*) and inert inertodetrinite (19 - 28 *vol. %, mmb*) were found to be most dominant in all the samples. Reactive semifusinite content was low: ≤ 14 *vol. %, mmb* in all four samples. Visible minerals under the microscope were in the range of 15 to 22 *vol. %, mmb* for the four coals, which showed a relative similarity to the ash content from proximate analysis except for coal C2 with lower visible minerals and higher ash content. This was probably due to its high content of the denser inertinite maceral and some maceral-mineral associations that may have introduced some problems in the identification of the mineral grains (Kruszewska, 2003). Total reactives, which refers to the maceral constituents that possess the propensity to react to heating, ranged from 35 to 44 *vol. %, mmb* for all the coal samples. Kaitano (2007); Everson *et al*. (2008b); and Phiri (2010) reported similar findings.

3.7.5.3 Microlithotype Analysis of Parent Coals

Microlithotypes refers to the association of macerals within the coal matrix and is analysed using a greater number of points (approximately 500) than are used the maceral analysis. (Cameron and Hunt, 1985; Falcon and Snyman, 1986; Snyman, 1989). This was done for the sake of completeness of petrographic data as well as for a better understanding of the subsequent chars properties. It is well known that the association and specific interactions of the different maceral components has a significant influence on the properties of the resultant chars after pyrolysis (Falcon and Snyman, 1986; Tsai and Scaroni, 1987; Cloke and Lester, 1994; du Cann, 2008). Analysis of the different microlithotypes present in each of the four coal samples was conducted in accordance with ISO 7404 - 4 (1998), and the results are presented in Table 3.19.

The proportion of pure vitrinite, vitrite (vitrinite > 95%) was generally low (< 13 *vol. %, mmb*) in coals B, C and D2 and just 2 *vol. %, mmb* in coal C2. Pure inertinite in the form of inertite (inertinite > 95%), however, accounted for > 32 *vol. %, mmb* of the coal macerals, with the highest concentration of 59 *vol. %, mmb* observed in coal C2. None of the four coals exhibited the presence of pure liptinite- liptites (liptinite > 95%) within the coal matrix. Apart from coal C2 with a substantially low intermediate maceral (bi-macerals and tri-macerals) volume (8 *vol. %, mmb*), the other three coals: B, C and D2 have maceral mixture concentrations of between 21 to 27 *vol. %, mmb*.

Table 3.19: Microlithotype analysis of coal sample (*vol. %,mmb*).

	Pure Mono-macerals (%)			Intermediates macerals/ maceral mixtures (%)				Carbominerite (%)	Minerite (%)	Total (%)
				Bi-macerals			Tri-macerals			
Coal ID	Vitrite	Liptite	Inertite	Clarite	Durite	Vitrinertite	Tri-macerite			
B	13	0	32	3	5	11	8	19	9	100
C	11	0	29	2	5	8	6	26	13	100
C2	2	0	59	0	2	3	3	24	7	100
D2	8	0	40	1	6	8	6	22	9	100

NOMENCLATURE:

Vitrite : Vitrinite > 95%

Liptite : Liptinite > 95%

Inertite : Inertinite > 95%

Clarite : Vitrinite + Liptinite > 95%

Durite : Inertinite + Liptinite > 95%

Vitrinertite : Vitrinite + Inertinite > 95%

Tri-macerite : Vitrinite, Inertinite, Liptinite > 5%

Carbominerite : Total inorganic/ organic microlithotypes

Minerite : > 60 vol. % minerals

Significant differences were not observed in the carbominerite (mineral-maceral associations) and minerite (mineral-rich particles) relative amounts in the four samples with values ranging from 19 to 26 *vol. %, mmb* and 7 to 13 *vol. %, mmb* respectively. This correlates well with the ash content of the four coals from proximate analysis where no sharp distinction was observed. There is a good agreement between this result and the observations of Kaitano (2007) and Phiri (2010).

3.7.5.4 Carbominerite and Minerite Analysis of Parent Coals

Carbominerite and minerite analyses were conducted for the purpose of completeness of petrographic information and to give an insight into the mineral associations and deportments with the macerals, both within the parent coals organic matrix, and the visible minerals (Everson *et al*., 2008a). Furthermore, it was used to validate other results relating to the mineral matter and ash components of both coal and char samples. While the carbominerites refers to minerals associated with the macerals (coal organic matrix), the minerites are the dispersed inorganic matter in the coal (Falcon and Snyman, 1982; du Cann, 2007; Everson *et al*., 2008b).

The relative abundance of the different carbominerites and minerites expressed as a percentage of the total carbominerite and total minerite are shown in Table 3.20. From these results, it is clear that the carbo-argilite and carbo-silicate mineral-maceral associations occur most commonly in all four coals as finely dispersed clay minerals. Carbonates were observed to be intimately mixed with the macerals in carbo-ankarite with its highest occurrence in coal D2, but its relative abundance in the coals are more contributed by the inorganic carbonate group.

The relative occurrence of carbo-pyrite is much the same for all the samples, indicative that most of the pyrite in the coals studied is associated with the organic components of the coal matrix. This confirms the result of increasing elemental sulphur contents from coals to char, reported in the ultimate analysis result (Table 3.8, Section 3.7.1). However, low occurrence of pyrite in the mineral-rich particles of coal C2 (0.43 *vol. %, mmb*) and coal D2 (0.11 *vol. %, mmb*) was observed. The clay and quartz group minerals occurred most commonly in all the coals and were frequently intimately associated with the coal macerals.

Carbo-argilite, carbo-silicate, clay and quartz groups are the most abundant carbominerites and minerites in the coals. This compares well with the predominance of kaolinite, clay and quartz groups in the XRD minerals (Section 3.7.2, Table 3.10) and the XRF analyses (Section 3.7.3, Table 3.11) results. Similar findings have been reported by Kaitano (2007), Matjie (2008) and Hattingh (2009) in their investigations on different South African coals.

Table 3.20: Carbominerite and minerite results as percentage of total carbominerite and minerite (*vol. %, mmb*).

Sample ID	**COAL B**	**COAL C**	**COAL C2**	**COAL D2**
Carbominerite				
Carbo-Argilite and Carbo-Silicate	89.5	84.6	79.2	72.7
Carbo-Pyrite	5.26	3.85	4.20	4.55
Carbo-Ankerite	5.26	11.5	16.7	22.7
Total Carbo- Minerite	100.02	99.95	100.1	99.95
Minerite				
Clay and Quartz Groups	66.7	76.9	71.1	88.8
Pyrite	11.1	7.70	0.43	0.11
Carbonate Group	22.2	15.4	28.5	11.1
Total Minerite	100	100	100.03	100.01

NOMENCLATURE:

Carbo-Argilite	:	Coal + 20 to 60 vol. % clay minerals.
Carbo-Silicate	:	Coal + 20 to 60 vol. % quartz
Carbo-Pyrite	:	Coal + 5 to 20 vol. % sulphides
Carbo-Ankerite	:	Coal + 20 to 60 vol. % carbonates
Carbo- Minerite	:	Total organic/inorganic microlithotypes
Minerite	:	> 60 vol. % minerals

3.7.5.5 General Condition of Coal Samples

From the petrographic analyses, the four coal samples were generally “fresh” in appearance. However, extensive cracks and micro-fissures were very common in the coal macerals (du Cann, 2007). This may have occurred during handling and preparation due to the brittle nature of the coal samples, which is characteristic of coals of this rank. Du Cann (2007) also noted that the tendency of a coal to crack may

lead to widespread development of low temperature thermal stress fractures (passive deflagration) on charring. The presence of deflagrating particles is an added advantage during combustion and gasification, as this result in increased fines, and thus higher surface areas for the reactions. Signs of severe weathering was quite often observed in coal D2 and occasionally seen in coals B, C, and C2. There is a lot of similarity in the general condition of the samples between the coals used in this study and those studied by Kaitano (2007); Everson *et al*. (2008b) and Phiri (2010).

3.7.6 Char Carbon Forms Analysis

Heat treatment of bituminous rank coals above 350 *°C* usually causes the maceral components: liptinite, vitrinites and some inertinites to soften, plasticise and expand (Falcon and Snyman, 1986; Tsai and Scaroni, 1987; Cloke and Lester, 1994; du Cann, 2008). Most of the inertinite components and minerals are not much affected. The applied heating rate and the final temperature attained are major determinants of the degree of expansion. Vesicles may also be formed in the reactive maceral components as volatiles are released (Cloke and Lester, 1994; du Cann, 2008). This leads to the formation of vacuoles and cellular structures resulting in porous chars. Chars of this type possess increased surface areas on which reaction occurs. Du Cann (2008) noted that most inertinites, and particularly fusinites do not soften, degasify or develop into porous structures. Instead, they form substantial dense chars with poor ignition and burn-out characteristics (Kaitano, 2007).

However, not all inertinites are “inert” and not all vitrinites are “reactive”. Cloke and Lester, (1994) in their review pointed out that some inertinite components are indeed “reactive”; noting that microlithotype association has a major influence on the propensity of these maceral components to react to heating. Inertinite maceral association with liptinites often results in the formation of porous chars during pyrolysis (Cloke and Lester, 1994).

The char carbon forms analysis was carried out on the basis of a 500 point-count in accordance with ISO 7404 - 3 (1994) and microscopic constituents of the samples were differentiated on the basis of their size; colour; reflectance; morphology; degree of anisotropy; and extent of devolatilisation (du Cann, 2008). The resulting char

carbon forms were classified according to the classification system proposed by du Cann (2008). An outline of this classification system is presented in Appendix A, while the result of the char carbon forms analysis is given in Table 3.21 on a mineral matter basis (*mmb*).

The following categories of char carbon form constituents based on the classification system were observed as reported by du Cann (2008). Photomicrographs of the observed components taken with a partially cross polarized reflected white light in oil immersion are also presented in Figures 3. 9; 3.10; and 3.11. It is worth noting that these photomicrographs are not peculiar to any of the chars, but provides a general illustration of observed characteristics of any of the four chars.

- **Category A1**: Chars with frequent tiny gas pores.

  These refer to "chars" that largely retain the original coal maceral structure with some fine pores. They originate from both coal- vitrinites and inertinites.

  i. Char carbon forms from coal vitrinites: These carbon forms are characterised by frequent tiny gas pores with no evidence of well developed devolatilisation vesicles. A depiction of this char carbon form is shown in the photomicrograph of Figure 3.9(i).
  ii. Char carbon forms from coal inertinites: These carbon forms originate from parent coal inertinites that have not softened, expanded or "opened up" to any appreciable degree on charring, causing them to largely preserve their original coal maceral shape and form. They are also commonly marked by tiny open pores resulting to some fine porosity. Features of this group of char carbon forms are shown in the photomicrograph of Figure 3.9(ii).

- **Category A2 and A3**: Char networks displaying varying degree of porosity.
  This category describes char made up of fine walled and thicker walled networks (Figure 3.10(i)). Char carbon forms exhibiting a fine walled network are derived from 'reactive-rich' coal macerals that had "opened up" to varying extents during charring and possesses high internal surface areas. Thicker walled networks originate from the 'inerts-rich' coal particles and are less porous.

Table 3.21: Char carbon forms analysis result (*vol. %, mmb*).

				Char ID			
Category	**Char carbon forms** (*vol. %, mmb*)	**Maceral of origin**	**Photomicrograph** (Fig.)	**B**	**C**	**C2**	**D2**
A 1 (i).	Char with frequent Tiny gas pores	Vitrinites	Fig. 3.9(i)	14	11	1	10
A1 (ii).	Dense Char with frequent Tiny gas pores	Inertinites	Fig. 3.9(ii)	27	24	31	22
A2.	More open network - Fine walled	Reactives	Fig. 3.10(i) (above)	7	8	6	4
A3.	More open network - Thicker walled	Inerts	Fig. 3.10(i) (below)	24	22	20	28
B7.	"Coke"- Isotropic thick walled	Vitrinites	Fig. 3.10(ii); 3.10(iii)	6	5	1	4
D12.	Partially reacted macerals - from coal	-	Fig. 3.10(iv); 3.10(v); Fig. 3.10(vi); 3.11(i)	1	1	17	2
E13.	Inorganic matter - from Coal	-	Fig. 3.11(v); 3.11(vi)	21	29	24	30
	Total (*vol. %, mmb*)			100	100	100	100

Groups A and B : Very highly reflecting, oxidation restricted

Group C : Relatively low reflecting, exhibiting oxidation rims

Group D : Low reflecting little or no change

Anisotropic Exhibiting optical properties of different values when viewed under crossed Nicols.

Isotropic Exhibiting optical properties that are the same in all directions when viewed under crossed Nicols.

- **Category B4 - B7**: Coke forms

  These char carbon forms originate from the pure vitrinite mono-maceral (vitrite) of the parent coals. Due to the fact that vitrinites and other reactive macerals soften and degasify during the charring process, pores and vacuoles are formed. These are visualised in Figure 3.10(ii). As the released gases within the pores and vacuoles increase in volume because of temperature effects, the softening walls expand giving rise to an increase in volume and surface area in the material. The "coke" identified in the char samples is of isotropic form, specifically Category B7, and exhibits substantially well developed devolatilisation vesicles and most usually quite thick "coke" walls which are again frequently marked with very fine-sized open pores. A typical highly porous isotropic coke char carbon form from reactives is shown in the photomicrograph of Figure 3.10(iii). None of the other coke categories: fine and medium "coke"; circular anisotropic and "coke"; incipient anisotropic "coke" (Category B4 - B6) were identified in any of the char samples.

- **Category C8 - C10**: Oxidation effects.

  Evidence of oxidation on the maceral components are usually characterised by the occurrence of dark rims and zones on particle edges around gasification pores. This was not observed on any of the four char samples.

- **Category D11**: Unaffected coal.

  Unaffected coal refers to materials in the parent coals unaffected by heat and was not encountered in any of the chars. Vitrinites in this category usually exhibit typical bituminous Medium Rank C reflectance ranges.

- **Category D12**: Partially reacted macerals.

  Materials classified under this category display reflectance levels above those of the parent coal vitrinites, but quite lower than those of the fully charred components. Partially reacted macerals are usually pitted with intermediate reflectivities in the range of 1% - 4 *Rr%*. This is an indication of limited devolatilisation and porosity is relatively poorly developed. The photomicrographs presented in Figures 3.10(iv), (v), and (vi) and 3.11(i) are good illustrations of char carbon forms associated with partially reacted macerals.

- **Category E13**: Visible minerals from parent coal.

  Category E13 (Visible minerals from parent coal) refers to the inorganic material derived from the parent coal and was identified in substantial quantities (21 - 30 *vol. %, mmb*) in all the char samples. Figures 3.11(v) and 3.11(vi) are good description of char form containing visible minerals.

  Neither inorganic matter derived from other sources (Category E14), nor process derived depositional carbon (Category F15) were observed in any of the char samples.

- **General condition of the chars**

  Depreciated organic materials, cracks and fissures were observed as a common feature in all the four char samples. These are due to thermal stress fracturing coupled with passive deflagration (du Cann, 2008). Severe weathering often observed in the parent coals may have also contributed to the depreciation of the organic materials in the subsequent chars.

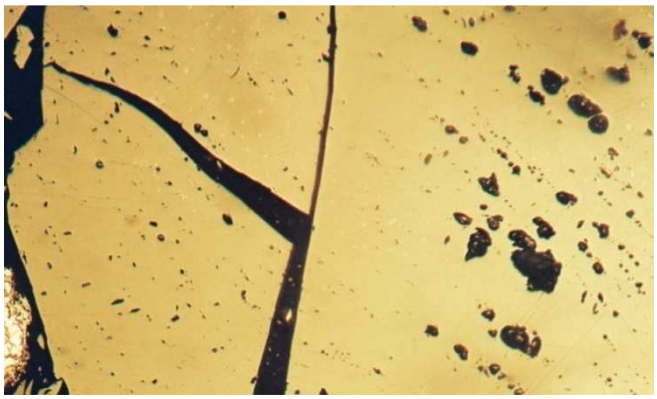

(i) Category A1: Char with frequent tiny gas pores from vitrinite which displays no major in change in original parent coal maceral structure

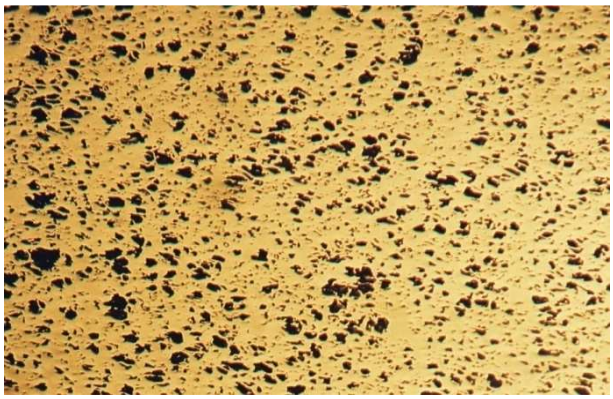

(ii) Category A1: Dense char from inertinite which has not “opened up” and increased porosity

Figure 3.9: Photomicrographs of different categories of char carbon forms (du Cann, 2008) (Magnification=2×10^5).

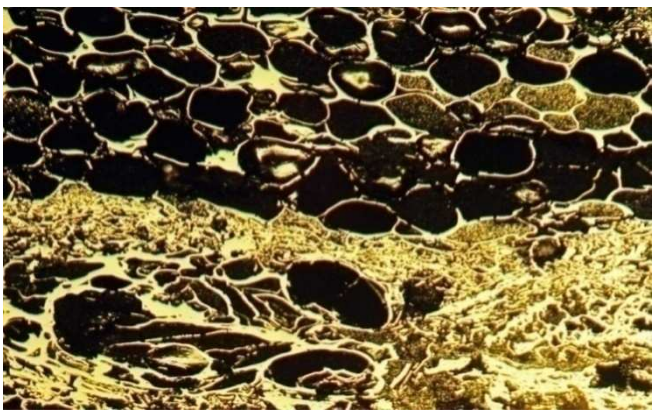

(i) Category A2: Fine walled from reactives-rich parent coal macerals (above); Category A3: Relatively thicker walled from inert coal macerals (below)

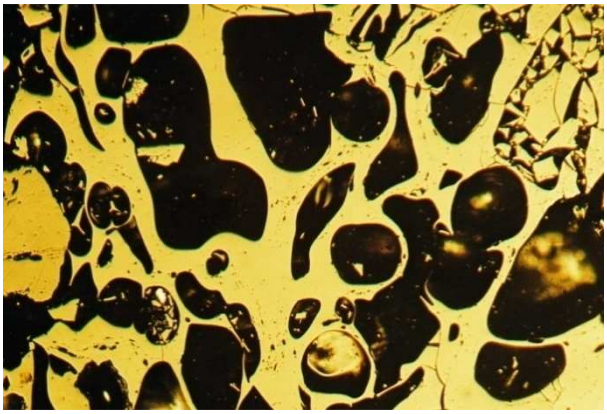

(ii) Category B7: Isotropic "coke" from vitrinite in the parent coal with well developed devolatilisation pores

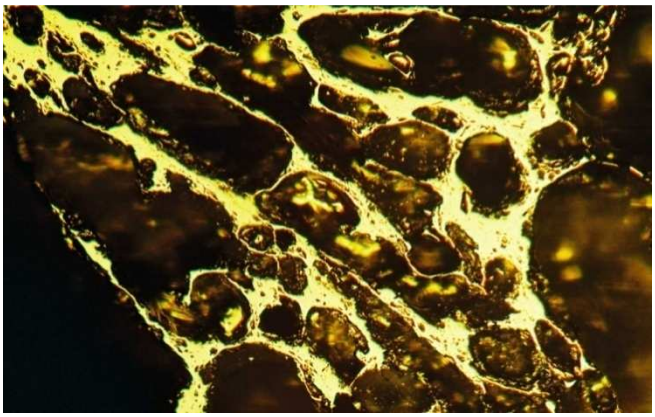

(iii) Category B7: Highly porous isotropic "coke" formed from reactives (i.e., vitrinite, liptinite, and reactive inertinite) in the parent coal

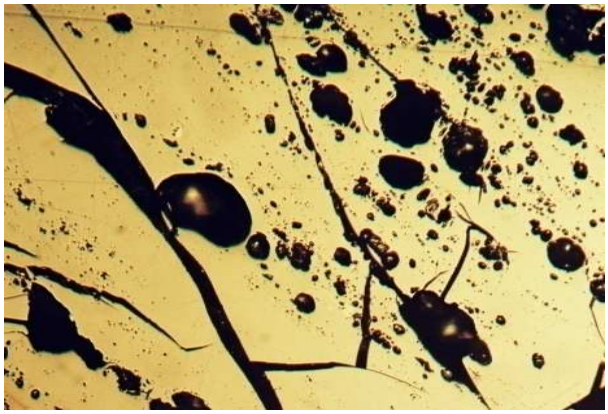

(iv) Category D12: Partially reacted vitrinite-Restricted devolatilisation

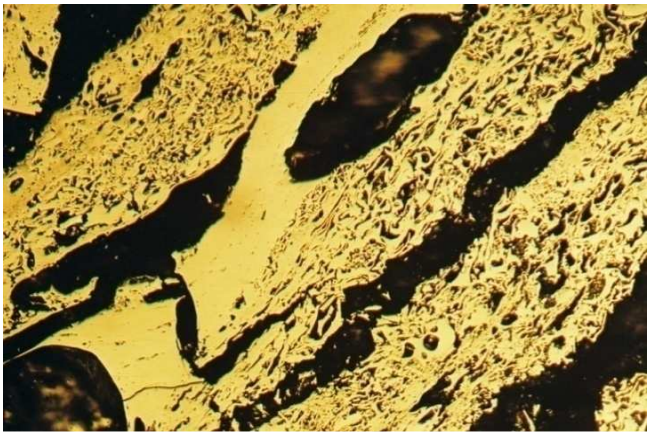

(v) Category D12: Partially reacted particle showing thermal stress fractures but little change in maceral structure and limited gas pore formation

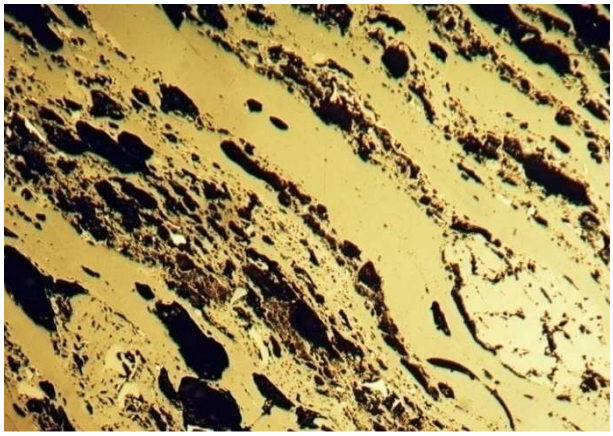

(vi) Category D12: Maceral bands with fine clay inclusions displaying little in change structure

Figure 3.10: Photomicrographs of different categories of char carbon forms (du Cann, 2008) (Magnification=2×10^5).

(i) Category D12: Fusinite showing deformation due to compression but no increase in porosity

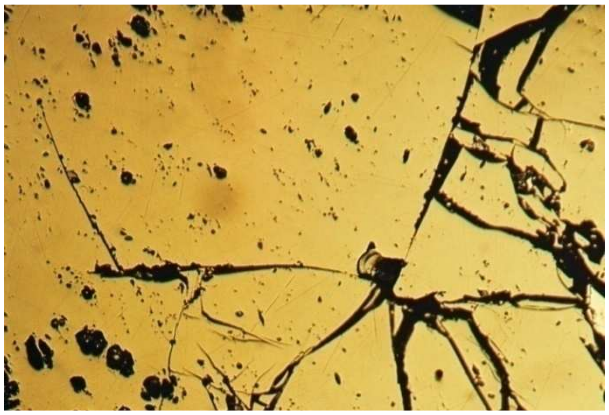

(ii) Extensive cracking in vitrinite but little change in maceral structure

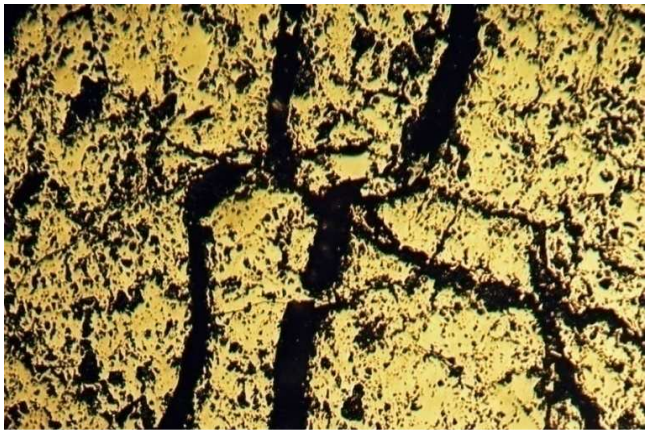

(iii) Char from inertinite displaying severe fissuration

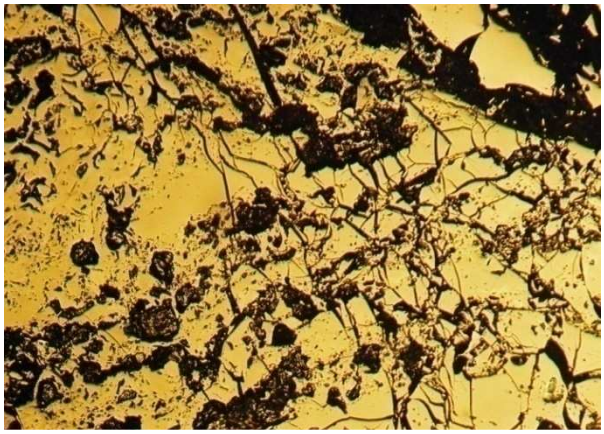

(iv) Inertodetrinites showing "passive deflagration" and disintegration giving rise to increased surface area

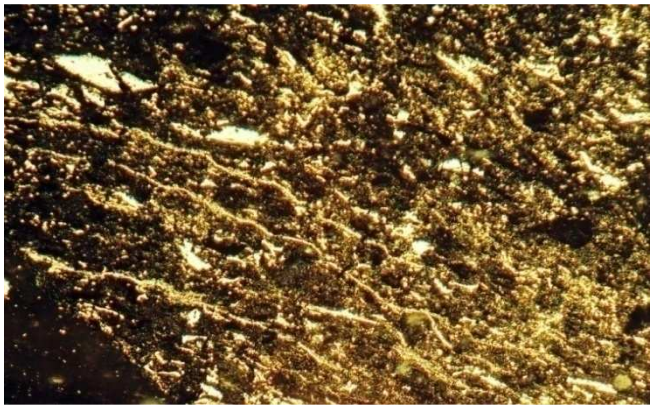

(v) Fine inertinite particles associated with clay minerals from carbominerite in the parent coal

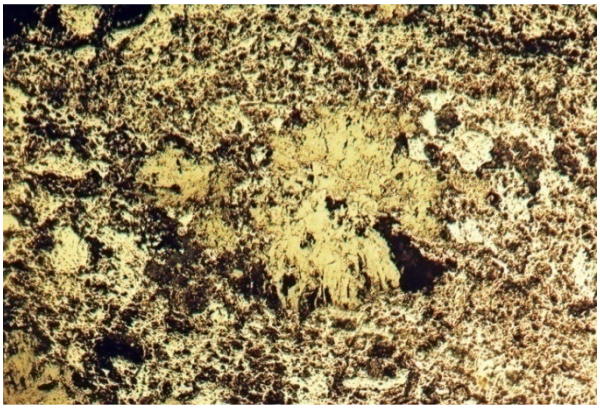

(vi) The remains of carbonates inter-grown in inertinite

Figure 3.11: Photomicrographs of different categories of char carbon forms (du Cann, 2008) (Magnification=2×10^5).

From the summary given in Table 3.21, all the four char samples show varying contributions of char carbon forms resulting from different macerals that substantially corresponds to the proportion of such macerals in the parent coals. It is also evident that there is a larger abundance of char carbon forms from coal inertinites (Category A1 and A3) in all the chars. Category A1 char forms were most abundant in the char samples, with chars with tiny gas pores from inertinites contributing between 22 - 31 *vol. %, mmb*. Thicker walled more open network char forms from coal inerts (Category A3) was next in abundance and were considerably high in all the char samples ranging in value from 20 *vol. %, mmb* in char C2 to 28 *vol. %, mmb* in char D2. The proportion of chars with frequent tiny gas pores from vitrinites ranged from 10 - 14 *vol. %, mmb* in char B, C and D2 with an exceptionally low value for char C2 at just 1 vol. %. Fine walled more open network char carbon forms from coal reactive macerals (Category A2), though low in abundance, was much the same in all the chars (4 - 8 *vol. %, mmb*). Minor proportions of isotropic "coke" derived from vitrinites (Category B7) were identified in approximately the same amount in chars B, C and D2 at 6, 5 and 4 *vol. %, mmb* respectively, with an exceptionally low value yet again for char C2 at 1 *vol. %, mmb* only.

The very low concentration of char forms from coal reactives and vitrinites in coal C2 is a good indication that it may be the least reactive of all the chars. Partially reacted macerals from coal (Category D12 char carbon forms) was observed to be high in coal C2 at 17 *vol. %, mmb*, but minimal in chars B, C and D2 at < 2 *vol. %, mmb*. It is again suspected that the relatively large amount of partially reacted maceral in char C2 may have caused its very low concentration of Category A1 and B7 char carbon forms. The volume of inorganic matter derived from coal (Category E13) was high (21 - 30 *vol. %, mmb*) in the samples, which is a good corroboration of the high ash content from the proximate analysis results of the coals and respective chars. Char D2 containing the highest amount of ash (36.8 *wt. %, db*) from proximate analysis, has the highest proportion of Category E13 char carbon forms, while char B with the lowest ash content (28.8 *wt. %, db*) was marked with the lowest volume of inorganic materials from coal.

The char carbon forms from: fine and medium "coke"- circular anisotropic (Category B4- 6); "oxidised" from inertinites, vitrinites and low reflecting networks (Category

C8-10); "unaffected" original coal vitrinites and inertinites (Category D11); inorganic matter derived from other sources apart from coal (Category E14); and process derived depositional carbons (Category F15), were not observed on any of the samples and thus were not reported in Table 3.21.

Comparisons were made of the total reactive and inert macerals of the parent coals and the total reactive and inert components and/or char carbon forms of the chars. It is generally accepted that the total reactive components of coal comprises of total liptinite, total vitrinite, reactive semifusinite and reactive inertodetrinite, while inert maceral components are made up of inert semifusinite, inert inertodetrinite, fusinite/secretinite and micrinite (Su *et al*., 2001; Helle *et al*., 2003; Kaitano, 2007; du Cann, 2007 and 2008; Phiri, 2010).

In the context of this study, total reactive char carbon forms were considered to encompass char carbon forms with frequent tiny gas pores from vitrinite (Category A1(i)); fine walled more open network char carbon forms from reactives (Category A2); and isotropic coke from vitrinites (Category B7). Total inert char components include dense char carbon forms with tiny gas pores from inertinite (Category A1(ii)) and thicker walled more open network from inerts (CategoryA3). Thus:

$$TRC_{COAL} = TL + TV + RSF + RINT \tag{3.13}$$

$$TRC_{CHAR} = Cat.(A1(i) + Cat.A2 + Cat.B7 \tag{3.14}$$

and,

$$TIC_{COAL} = F + SEC + MIC + ISF + IINT \tag{3.15}$$

$$TIC_{CHAR} = Cat.(A1(ii) + Cat.A3 \tag{3.16}$$

A detailed summary of this comparison is presented in Table 3.22. Generally, more of the total reactive components (*TRC*) in the coals were lost in the transition to chars than the total inert components (*TIC*). The *TRC* experienced percentage losses of 38.6, 36.8 and 48.6% in samples B, C and D2 respectively, while an unprecedented 76.5%

loss was observed in sample C2. This unexpectedly high loss in *TRC* may be due to the presence of partially reacted macerals of about 17 *vol. %, mmb* in char C2, which was neither classified as part of the *TRC* nor *TIC*. Most of the *TRC* losses are in the form of volatiles after softening and expansion of the original coals (Tsai and Scaroni, 1987), and of passive deflagration during devolatilisation (Kaitano, 2007). The resultant higher density and higher maceral reflectance of the chars are also evidence of the loss of lower molecular weight *TRC* components and/or conversion to higher molecular weight, more aromatic and denser *TIC* components in the transition from coals to chars (Cloke and Lester, 1994; du Cann 2008).

Table 3.22: Total reactive and inert components of coal and char samples (*vol. %, mmb*)

Components / Sample ID	**Total Reactive Components (*TRC*)- Coal and Char**							
	Coal B	**Char B**	**Coal C**	**Char C**	**Coal C2**	**Char C2**	**Coal D2**	**Char D2**
Total Vitrinite	28	-	19	-	3	-	13	-
Total Liptinite	3	-	3	-	3	-	4	-
Reactive Semifusinite	7	-	7	-	14	-	10	-
Reactive Inertodetrinite	6	-	9	-	14	-	8	-
Category A1 (i) Char forms[1]	-	14	-	11	-	1	-	10
Category A2 Char forms	-	7	-	8	-	6	-	4
Category B7 Char forms	-	6	-	5	-	1	-	4
Total	44	27	38	24	34	8	35	18
% loss of *TRC* in chars (%)	**38.6**		**36.8**		**76.5**		**48.6**	
	Total Inert Components (*TIC*)- Coal and Char							
Inert Semifusinite	13	-	13	-	17	-	19	-
Fusinite/ Secretinite	3	-	3	-	4	-	4	-
Micrinite	1	-	1	-	2	-	1	-
Inert Inertodetrinite	24	-	24	-	28	-	19	-
Category A1(ii) Char forms	-	27	-	24	-	31	-	22
Category A3 Char forms	-	24	-	22	-	20	-	28
Total	41	51	41	46	51	51	43	50
% gain of *TIC* in chars (%)	**24.4**		**12.2**		**0.00**		**16.3**	

[1]- See sections 3.7.5.2 and 3.7.6 and Appendix A for descriptions

The majority of the inert components of the coal rarely soften, expands or "open up" to any appreciable extent on charring (du Cann, 2008). They therefore retain most of the features of the parent coal macerals. Unlike the *TRC*, the total inert components (*TIC*) of the samples generally exhibited gross gains in *TIC* between 12.2 and 24.4%, except for sample C2, with neither loss nor gain in *TIC* (0%). The gains in *TIC* in samples B, C, and D2, imply that some of the *TRC* of the parent coals may have been transformed to inert components char carbon forms by the pyrolysis reaction. The observation of neither loss nor gain in *TIC* in Sample C2 suffixes that the parent coal inert macerals were not affected by the charring process; which is generally unrealistic. This can, once more, be attributed to the high volume of partially reacted maceral char carbon form in sample C2 that was not identified as part of either the *TRC* or the *TIC* in the subsequent char carbon forms.

Further illustrations are shown in Figure 3.12. A comparison of the parent coal vitrinites and inertinites with their resultant specific char carbon forms was made and the result is a decreasing concentration in the transition from coals to chars for all the samples (Figure 3.12(i) and 3.12(ii)). The *TRC* and *TIC* of the parent coals, and subsequent chars, were also compared graphically in Figure 3.13(i) and 3.13(ii). *TRC* decreased from coals to chars while an opposite trend was observed for the *TIC*, except for sample C2 (0%).

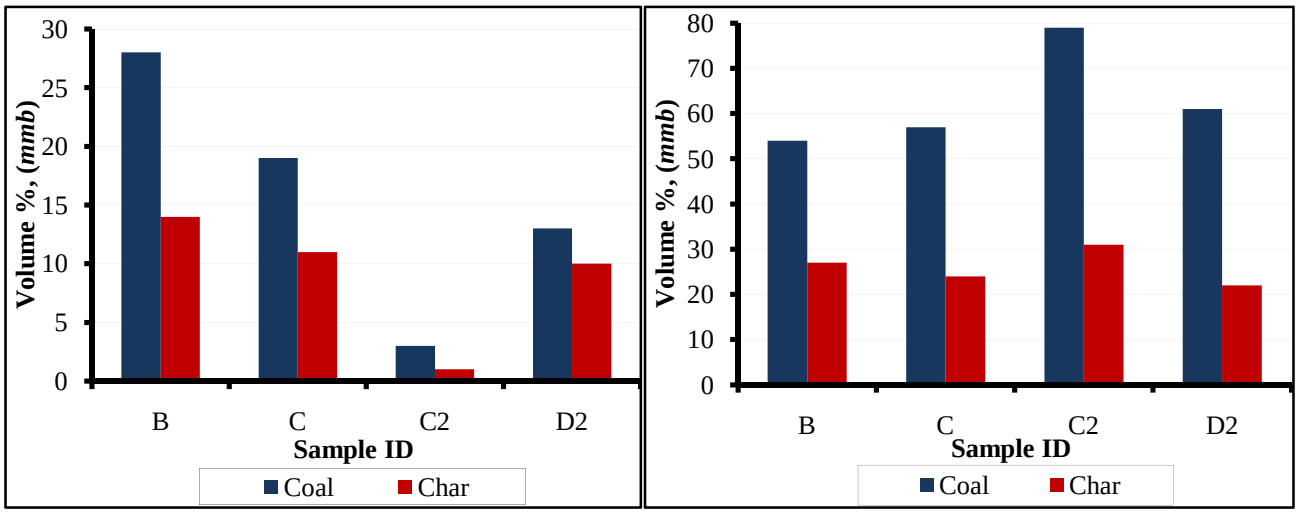

(i) Parent coal vitrinite and resultant Category A1 (i) char forms

(ii) Parent coal inertinite and subsequent Category A1 (ii) char forms

Figure 3.12: Comparison of parent coals macerals and their specific char carbon forms in the chars.

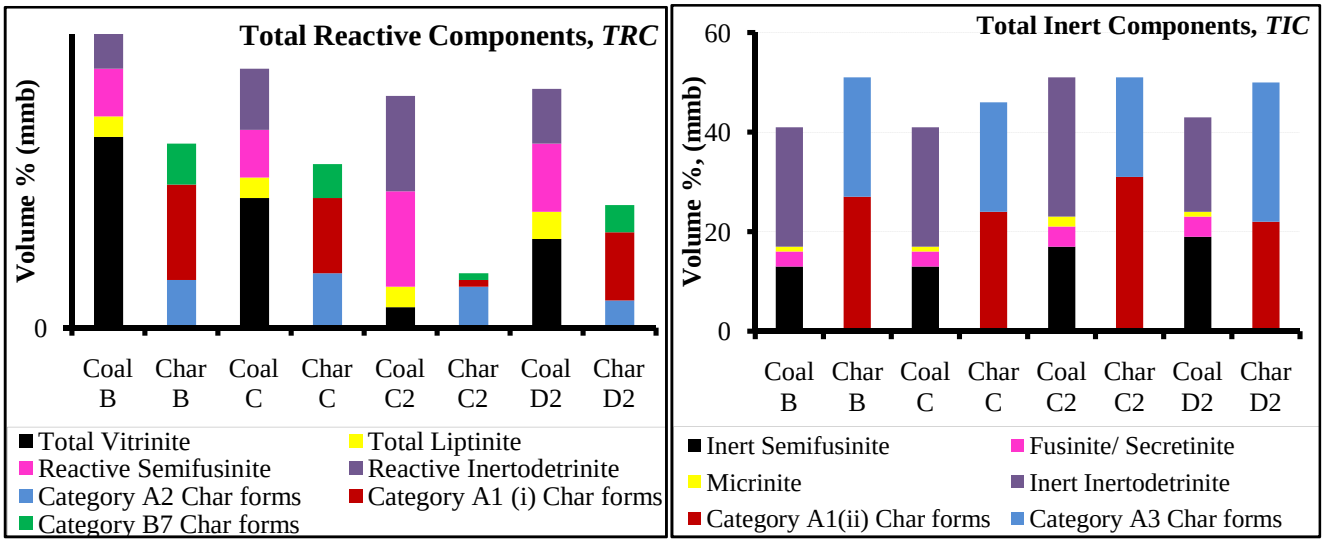

(i) Comparison of coals- and chars- *TRC* (ii) Comparison of coals- and chars- *TIC*

Figure 3.13: Comparison of the total inert and reactive components in the parent coals and the resultant chars.

3.7.7 Physical Structural Analysis: Coal and Char Samples

Characterisation of the physical structural properties of the samples was carried out on both coal and char samples. Results of the skeletal density of the samples are shown in Figure 3.14 and Table 3.23.

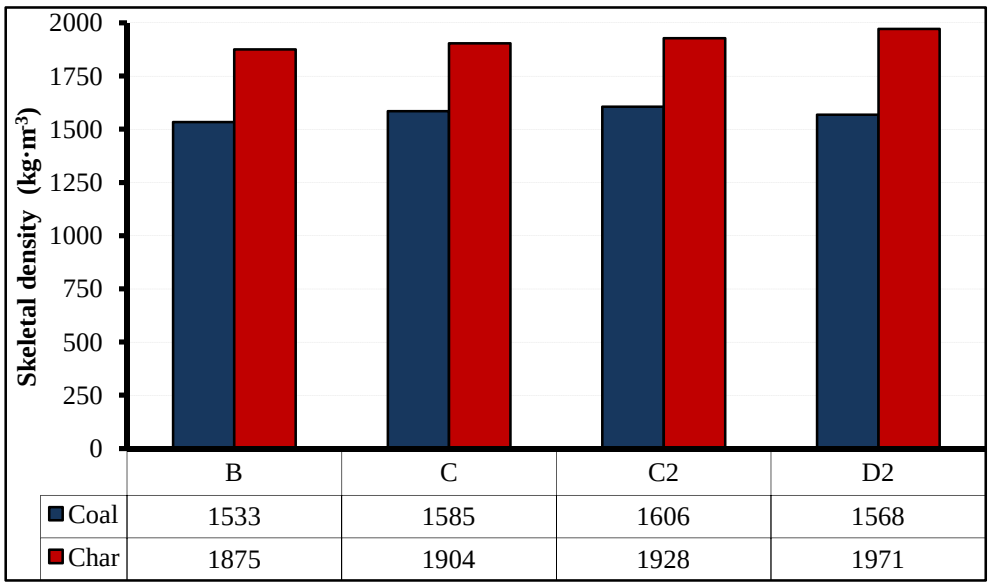

	B	C	C2	D2
Coal	1533	1585	1606	1568
Char	1875	1904	1928	1971

Figure 3.14: Skeletal density of coal and char samples.

Even though the skeletal density of the coal samples did not show much variation, with their values between 1533 to 1606 $kg \cdot m^{-3}$, it is important to note that it increases with increasing inertinite content, and decreases with increasing vitrinite content of the coals. The higher density observed in coal C2 was thus suspected to be due to its large content of high density inertinite macerals (79 *vol. %, mmb*) and lower volatile matter content (18.9 *wt. %, db*). These correlate well with the results obtained by Senneca *et al*. (1998) and Hattingh (2009) in their various investigations of some South African coals. An increase in skeletal density (1875 - 1971 $kg \cdot m^{-3}$) was observed in the chars. This is expected since the charring process evacuates volatiles and low molecular mass species from the coals, leaving behind heavier carbon-rich and mineral-concentrated chars. The high skeletal density of 1971 $kg \cdot m^{-3}$ exhibited by char D2 can be attributed to its high ash content (36.8 *wt. %, db*), in addition to its high volume of inertinite char carbon forms. Unlike the parent coals, no specific trend was found between the resultant char carbon forms and the skeletal density of the chars which varied only slightly.

The micropore surface area for both coal and char samples was determined according to the Dubinin-Radushkevich (D-R) method using carbon dioxide as adsorption gas (Anderson *et al*., 1965; Walker and Kini, 1965; Walker *et al*., 1988). The results of these analyses are given in Figure 3.15. A detailed summary including mono-layer pore volume, determined by the Dubinin-Radushkevich method and average micropore diameter, determined by the Horvath-Kawazoe method (Horvath and Kawazoe, 1983; Jaroniec *et al*., 1996; Kowalczyk *et al*., 2002) are presented in Table 3.23.

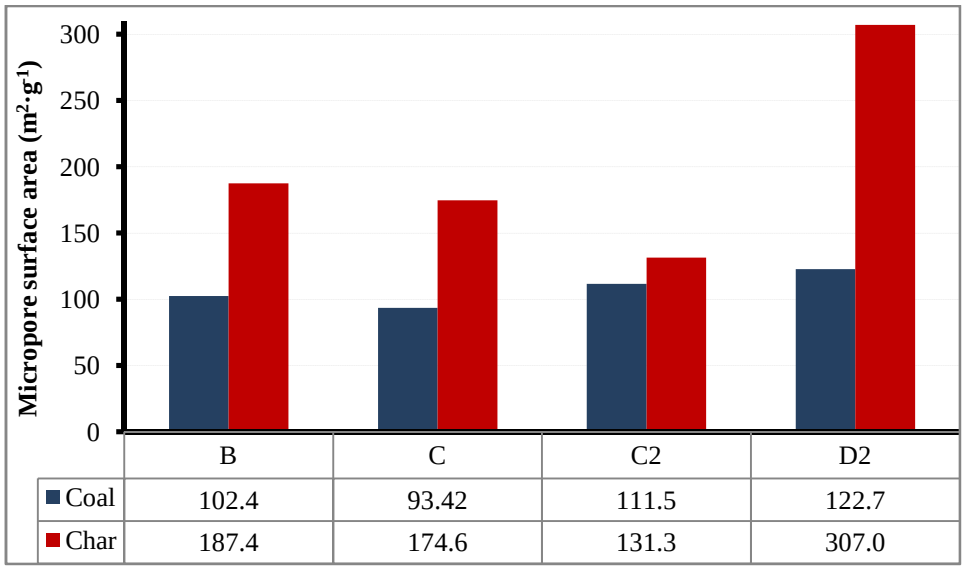

	B	C	C2	D2
Coal	102.4	93.42	111.5	122.7
Char	187.4	174.6	131.3	307.0

Figure 3.15: Micropore surface area of coal and char samples.

Table 3.23: Physical structural properties of coal and char samples.

Property / Sample ID	**Method Used**	**Coal B**	**Char B**	**Coal C**	**Char C**	**Coal C2**	**Char C2**	**Coal D2**	**Char D2**
Micropore surface area ($m^2 \cdot g^{-1}$)	D-R	102.4	187.4	93.42	174.6	111.5	131.3	122.7	307.0
Mono-layer capacity ($cm^3 \cdot g^{-1}$)	D-R	22.42	41.02	20.45	38.22	24.4	28.75	26.87	67.20
Average micropore diameter (Å)	H-K	4.161	3.651	4.115	3.724	4.111	3.868	3.935	3.613
Micropore volume $x10^{-2}$ ($cm^3 \cdot g^{-1}$)	H-K	2.167	5.283	2.047	4.486	2.389	3.101	3.377	6.636
Skeletal (Apparent) density ($kg \cdot m^{-3}$)	HP	1533	1875	1585	1904	1606	1928	1568	1971
Porosity (%) ($D_p \leq 5$Å)	AD	2.882	9.970	2.906	8.247	3.346	5.188	5.424	12.75

NOMENCLATURE:

D-R : Dubinin-Radushkevich method

H-K : Horvath-Kawazoe method

HP : Helium Pycnometry

AD : CO_2 Adsorption data

The micropore surface areas of the coals did not exhibit much variation, with values ranging between 93.42 $m^2 \cdot g^{-1}$ for coal C and 122.7 $m^2 \cdot g^{-1}$ for coal D2. The softening, plasticizing, expansion and the release of volatiles from the parent coal (Falcon and Snyman, 1986; Tsai and Scaroni, 1987; Cloke and Lester, 1994; du Cann, 2008) during the charring process resulted in the opening of closed, blind and inaccessible pores (Laurendeau, 1978); formation of vacuoles, vesicles and cellular structures (Cloke and Lester, 1994; du Cann, 2008) and the enlargement of pores (micropores to mesopores and mesopores to macropore) (Laurendeau, 1978). The combined impact of these is an increase in surface area and porosity as observed in the chars. Unlike the parent coals, sharp differences were observed in the micropore surface areas of the chars. The micropore surface areas of char B and C were very close to each other at 187.4 and 174.6 $m^2 \cdot g^{-1}$. Char C2 exhibited a very low micropore surface area, resembling that of parent coal at 131.3 $m^2 \cdot g^{-1}$. This is possibly due to the large amount of inertinite maceral (not easily affected by heat) in the parent coal (79 *vol. %, mmb*), and the high volume of partially reacted macerals in the char (17 *vol. %, mmb*). Char D2 exhibited an exceptionally high micropore surface area of 307 $m^2 \cdot g^{-1}$ up from the 122.7 $m^2 \cdot g^{-1}$of the precursor coal. This may be due to its higher microporosity (Walker *et al*., 1988). The mono-layer capacity is a function of the surface area and accordingly varies with it. Phiri (2010) made similar findings. However, it was observed that the increasing order of the micropore surface area in the coals (coals C < B < C2 < D2), changed in the chars (chars C2 < C < B < D2). This shows that the parent coals are different to the subsequent chars in terms of porosity, although there is an inter-play of many factors as far as char properties are concerned (Franklin, 1951; Cloke and Lester, 1994; Davis *et al*., 1995; Russell *et al*., 1999; Lu *et al*., 2002a and 2002b).

It is generally accepted that carbon dioxide adsorption gives a better characterisation of micropores < 20 Å (Anderson *et al*., 1965; Walker and Kini, 1965; Walker *et al*., 1988) than does nitrogen adsorption (Garrido *et al*., 1987). This is due to the faster diffusion of carbon dioxide into finer micropores at 273 K than nitrogen at 77 K (Walker *et al*., 1988; Garrido *et al*., 1987). The adsorption isotherm plots of both coals and chars are shown in Figure 3.16. Comparison of the adsorption isotherms of the parent coals and the respective subsequent chars are further illustrated in Figure 3.17. The higher quantity of adsorbed CO_2 in the chars as compared to the coals is

indicative of the higher D-R micropore surface areas attained by the chars. Despite the fact that the micropore surface area of the chars increases with decreasing skeletal density with respect to chars B, C and C2; which was not observed for the parent coals. Char D2 was completely out of trend in this correlation and was thus, not reported in this dissertation.

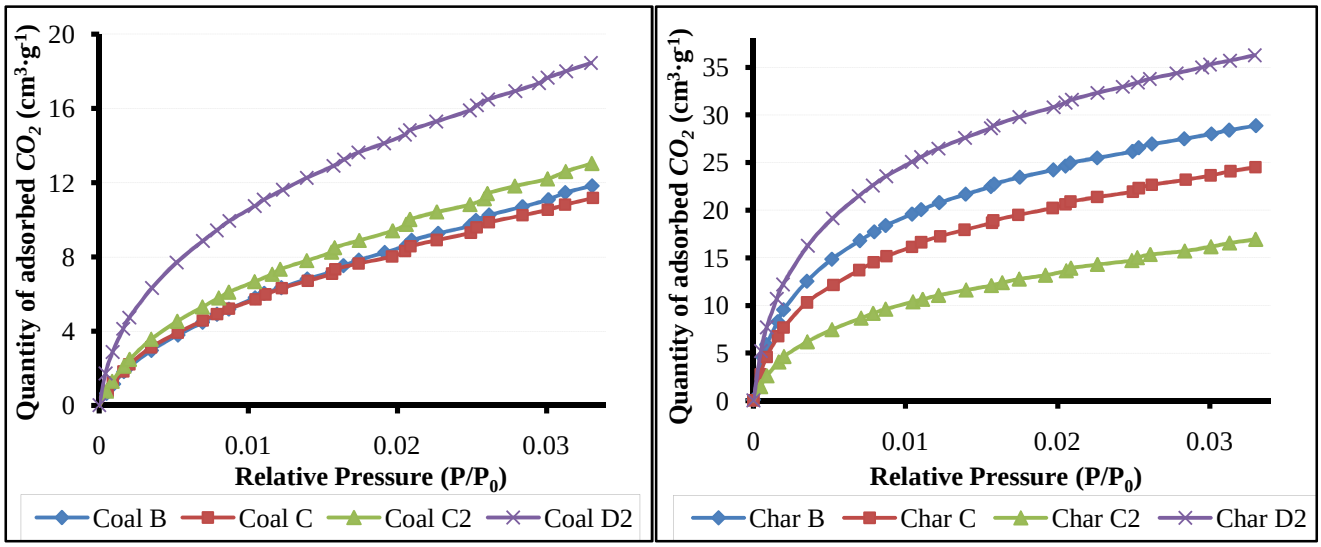

(i) CO_2 adsorption isotherm plots for coal samples (ii) CO_2 adsorption isotherm plots for char samples

Figure 3.16: CO_2 adsorption isotherm plots for coal and char samples.

The average micropore diameter as determined by the Horvath-Kawazoe method was found to generally decrease from the coals (3.935 - 4.161 Å) to the chars (3.613 - 3.868 Å). This is due to opening of closed and inaccessible micropores due to thermal treatment and the release of volatiles, while the highest value of 3.868 Å observed for char C2 may be attributed to the lowest volatile matter content of its parent coal (18.2 *wt. %, adb*) and the higher content of partially reacted macerals in the char. The pore volume (micropores: $D_p \leq 5$Å) (Micromeritics, 2006) increased from coals to chars and the increments are consistent with the increase in the micropore surface area. It can be seen from Table 3.23 that char D2 has the highest adsorbate pore volume, a good indication of its exceptional surface area with respect to the other three chars.

Micro-porosity of both coal and char samples ($D_p \leq 5$ Å) determined from CO_2 adsorption data show that the parent coals exhibited very little porosities (< 5.5%) with coal B having the lowest porosity of 2.9%. Although porosity generally increased from coals to chars, porosity values of the chars are quite low as well. This

is probably due to the high inertinite maceral content of the parent coals (Laurendeau, 1978; Falcon and Snyman, 1986; Snyman and Botha, 1993), and the relatively high *TIC* components in the chars (Cloke and Lester, 1994; du Cann, 2008). The low porosity of char C2 is probably due to the precursor coal's very low volatile matter content (Tsai and Scaroni, 1987; Cloke and Lester, 1994) and a higher volume of dense and partially reacted maceral content in its char carbon forms. It was also found that the increasing order of porosity in the coals (coal B < C < C2 < D2) changed in the chars (char C2 < C < B < D2). This further strengthens the fact that there are variations between coal and char properties with respect to porosity, even though the later is derived from the former.

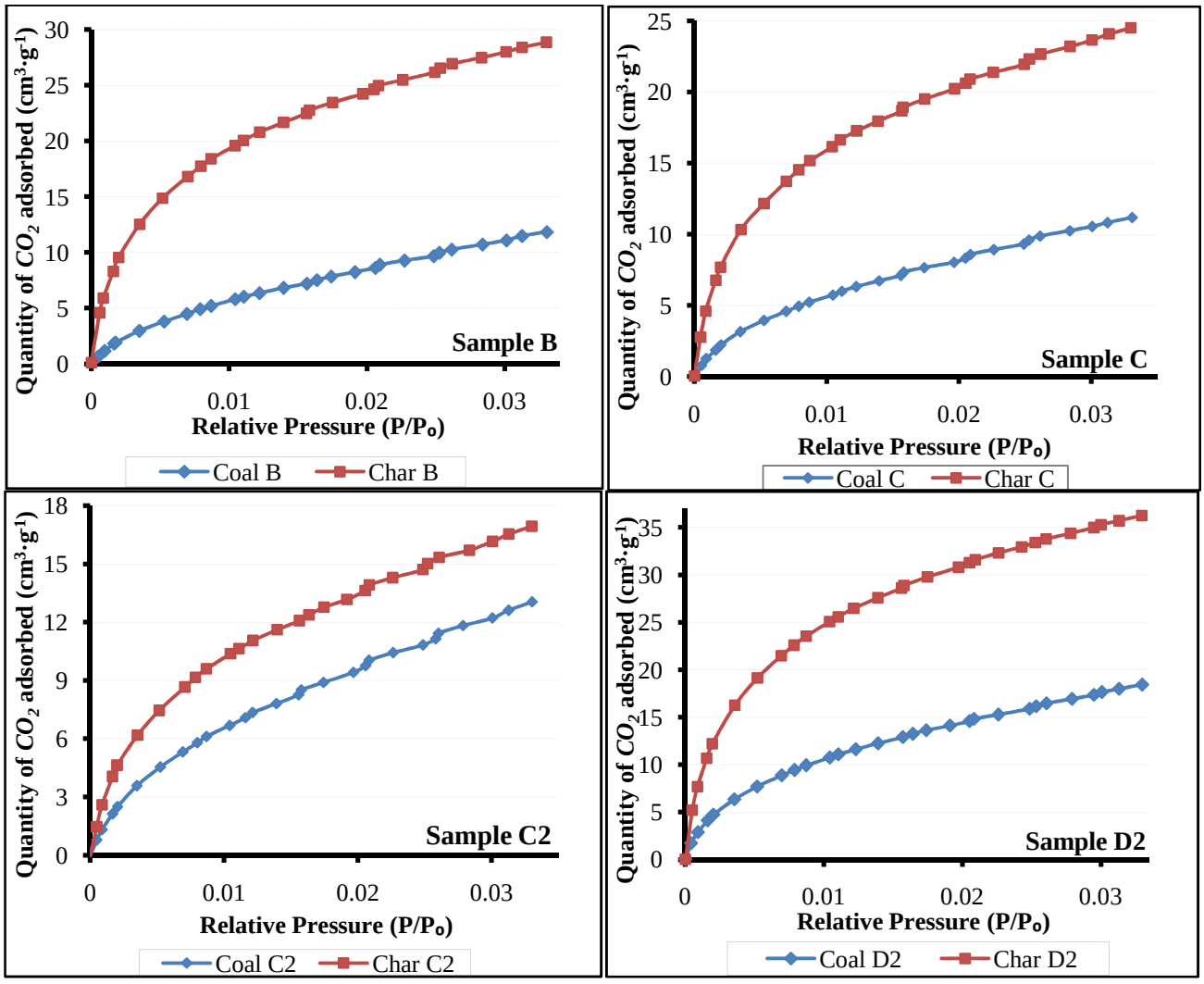

Figure 3.17: Comparison of the CO_2 adsorption isotherm plots for coals and chars: B, C, C2 and D2.

3.8 Summary

Analysis of the char yield after char production clearly shows that the mass of the resultant char produced from each batch of the process is equivalent to the sum of the fixed carbon and ash contents of the parent coals. This clarifies that, the moisture and volatile matter contents of the coals are almost completely evacuated by the charring process.

The original four coals were characterised as high ash coals, with ash contents in the range of 26.7 to 34.5 *wt. %, db*, while the respective chars exhibited higher ash content values after pyrolysis with values between 28.8 to 36.8 *wt. %, db*. All the coal samples were relatively low in volatile matter (< 24 *wt. %, db*), which was significantly driven off during the charring process, with the chars having VM values between 0.81 to 3.30 *wt. %, db*. It should be noted that, although significant devolatilisation took place during char production, most of the char carbon forms (especially the 'inert' char carbon forms) did not increase in porosity to any appreciable degree under the petrographic miscroscope. Moisture content went down to ≤ 1.58 *wt. %, adb* in the chars from the precursor coals' values of 3.40 to 6.50 *wt. %, adb*; while fixed carbon in the coals (42.9 - 49.4 *wt. %, db*) went up to values between 60.2 to 69.4 *wt. %, db* in the chars. The gross calorific value of the parent coals, though low, was found to be approximately the same within the small range of 18.1 $MJ \cdot kg^{-1}$ - 21.4 $MJ \cdot kg^{-1}$.

Elemental carbon content was the same for coals B, C and C2 at 73.1 *wt. %, daf*; while coal D2 has a lower value at 68.1 *wt. %, daf*. The elemental hydrogen-carbon and the oxygen-carbon ratios for the samples were rather low and were reflected in the higher aromaticity and lower fraction of amorphous carbon in both coals and chars.

From petrographic analysis, the mean vitrinite reflectance of the parent coals ranged from 0.56% to 0.75 %*Rr*, hence the coal samples were characterised as bituminous, medium rank C (coals B, C and C2) and bituminous, medium rank D coals (coal D2), according to the ISO 11760 method (2005). The four coals' total maceral reflectance scans had values ranging from 1.15 to 1.63 *Rsc%*. The devolatiliastion process shifted the total maceral reflectance of the subsequent chars to substantially higher values

within the narrow range of 4.43 to 5.28 *Rsc%*. The coals were characterised as inertinite-rich with inertinite maceral content between 54 to 79 *vol. % mmb* and inertinite-vitrinite ratios of: 1.93, 3.00, 26.3, and 4.70 respectively for coal B, C, C2 and D2.

It was observed from the microlitotype analysis, that the pure mono-maceral, inertite was the dominant maceral component in all four parent coals (>32 *vol. %, mmb*), with a value as high as 59 *vol. %, mmb* for coal C2. The liptinite mono-maceral, liptite was not identified in any of the coal samples.

It was deduced from the carbominerite and minerite analysis that both organic and inorganic association of minerals existed with the macerals of the coal samples. The coal samples were pitted with higher fractions of carbominerites (19 - 26 *vol. %, mmb*) relative to the minerite fraction at 7 - 13 *vol. %, mmb*. The carbominerite and minerite analysis results were consistent with the results from the XRD mineral analysis of the parent coals and the XRF ash analysis of the chars, with the dominant presence of kaolinite, clay and quartz species in all the samples.

The transition from coals to chars at 900 *°C* led to the formation of various char carbon forms in the chars. Coal reactive macerals formed minor proportions of isotropic “coke” and fine char networks, while some vitrinites and the majority of the coal inertinites resulted in denser char carbon forms, and these formed a greater volume of the subsequent chars having a marked increase in random maceral reflectance values. The total reactive components (*TRC*) generally decreased from coals to chars, with losses >36.5%. The total inert components (*TIC*) exhibited a gain in the transition from coals to chars (12.2 to 24.4% loss), except char C2 with 0% gain. This may have resulted from the conversion of some of the “reactive” macerals in the coals to inert char carbon forms during the char formation process.

Demineralisation of coals and chars prior to XRD carbon crystallite analysis gave higher demineralisation efficiencies for the parent coals (96.7 - 98.3%) than for the chars (89.1 - 93.3%). The XRD diffractograms of both the demineralised coal and char samples was observed to posses graphitic features characteristically similar to that of graphite by the presence of (*002*), (*10*), and (*11*) peaks.

With respect to the carbon crystallite analysis, it was observed that the chars possessed a more compact, better aligned and more structurally ordered carbon content than their respective original coals. Lattice parameters: crystallite height, L_c, and crystallite diameter, L_a, decreased, while the inter-layer spacing, d_{002}, increased from coals to chars. Thus the carbon structure of the chars was more condensed and smaller that that of the parent coals. Aromaticity was observed to increase, while the fraction of amorphous carbon decreased from coals to chars. It could also be inferred from the XRD carbon crystallite analysis results that the structural disorderliness of the chars increased in the order: Char C2 < Char C < Char B < Char D2. Hence, the degree of disorder index, *DOI*, decreased from char D2 down to char C2.

The charring process also impacted on the physical structural properties of the subsequent chars. The D-R micropore surface areas increased from values of 93.42 $m^2 \cdot g^{-1}$ to 122.7 $m^2 \cdot g^{-1}$ for the coals to 131.3 $m^2 \cdot g^{-1}$ to 307.0 $m^2 \cdot g^{-1}$ in the chars, while the H-K average micropore diameters decreased from coal to chars. Skeletal density was generally found to increase from coals (1533 - 1606 $kg \cdot m^{-3}$) to chars (1875 - 1928 $kg \cdot m^{-3}$) and was probably influenced significantly by the inertinite content of the parent coal. Apart from maceral content, ash content also affected the skeletal density as char D2 with the highest ash content exhibited the highest density. Char D2 also exhibited a considerably higher D-R micropore surface area with respect to the other chars.

Microporosity of both coals (2.882 - 5.424%) and chars (5.188 - 12.75%) were rather low, which can be attributed to the high volumes of total inert components (*TIC*) in both coals and chars. This is because *TIC*s do not react easily to heating. The high volume of partially reacted maceral (char carbon form) in char C2 (17 *vol. %, mmb*) and the parent coal's lower volatile matter content (18.2 *wt. %, adb*) may have contributed to its very low porosity with respect to the other chars. Average micropore diameter and micropore volume were observed to generally decrease from coals to the subsequent chars.

Mineral analysis by XRD showed that significant mineral interactions and transformations occurred in the coal to char transition at 900 *°C*. Out of 16 crystalline mineral phases identified in the coal and char samples, only quartz and calcite were observed in both the coals and chars. Kaolinite and quartz were the dominant mineral

phases identified in the coals, while quartz, cristobalite and microcline formed greater proportions of minerals in the char samples. However, significant variations were not observed in the relative abundance of the various mineral phases in the coals and respective chars as their values vary within a small range.

Ash components analysis revealed that SiO_2 and Al_2O_3 were the dominant inorganic species in the residual ash of the chars. Other inorganic species of catalytic importance detected in the ashes of the chars are: *Fe*-, *Ca*-, *Mg*-, *Na*- and *K*- species. The alkali index of the chars based on the detected inorganic components in increasing order of magnitude was: 2.55 for C2; 5.92 for char B; 6.15 for char C; and 7.17 for char D2.

On the condition analysis of the samples, the coal samples were found to be generally "fresh" in appearance, with frequent micro-fissures in macerals which are evidence of weathering. Cracks, fissures and deteriorated organic material were common in all four chars. These features common to the chars may be attributed to thermal stress fracturing and passive deflagration.

From the characterisation results, it was observed that, apart from the maceral contents and the inertinite-vitrinite ratios, coals B, C, and C2 did not exhibit sharp variations in their investigated properties, while coal D2 was significantly different. However, the subsequent chars exhibited substantial variations in both their chemical and physical structural characteristics. The increasing order of magnitude of the micropore surface area, microporosity, fraction of amorphous carbon, and the extent of disorderliness of the carbon crystallite all changed in the transition from parent coals to the subsequent chars. This shows that coals are comparatively different to the chars derived from them.